

AMERICAN UNIVERSITY OF BEIRUT

ASSESSING THE ROLE OF PCM AND WELL DESIGN IN
ENHANCING THE PERFORMANCE OF COAXIAL
GEOTHERMAL WELLS

by
JAMIL FADI EL MASRY

A thesis
submitted in partial fulfillment of the requirements
for the degree of Master of Science
to the Department of Mechanical Engineering
of the Maroun Semaan Faculty of Engineering and Architecture
at the American University of Beirut

Beirut, Lebanon
August 2023

AMERICAN UNIVERSITY OF BEIRUT

ASSESSING THE ROLE OF PCM AND WELL DESIGN IN
ENHANCING THE PERFORMANCE OF COAXIAL
GEOTHERMAL WELLS

by
JAMIL FADI EL MASRY

Approved by:

Dr. Elsa Maalouf, Assistant Professor
Bahaa and Walid Bassatne Department of
Chemical Engineering and Advanced Energy

Signature



Advisor

Dr. Alissar Yehya, Assistant Professor
Department of Civil and Environmental
Engineering

Signature

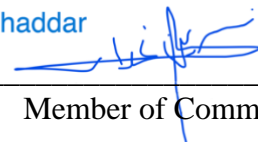


Co-Advisor

Dr. Nesreen Ghaddar, Professor
Department of Mechanical
Engineering

Signature

N. Ghaddar



Member of Committee

Dr. Fouad Azizi, Associate Professor
Bahaa and Walid Bassatne Department of
Chemical Engineering and Advanced Energy

Signature



Member of Committee

Date of thesis defense: August 23, 2023

AMERICAN UNIVERSITY OF BEIRUT

THESIS RELEASE FORM

Student Name: El Masry Jamil Fadi

I authorize the American University of Beirut, to: (a) reproduce hard or electronic copies of my thesis; (b) include such copies in the archives and digital repositories of the University; and (c) make freely available such copies to third parties for research or educational purposes:

- As of the date of submission
- One year from the date of submission of my thesis.
- Two years from the date of submission of my thesis.
- Three years from the date of submission of my thesis.



07/09/2023

Signature

Date

ACKNOWLEDGEMENTS

Foremost, I am grateful to God for giving me the strength and ability to complete my thesis.

I would like to express my sincere gratitude to my advisors Prof. Elsa Maalouf and Prof. Alissar Yehya who significantly contributed to my thesis with their motivation, enthusiasm, immense knowledge and caring. Their guidance, support, and patience were essential to the successful completion of this research.

I would like to extend my sincere thanks to my committee members Prof. Nesreene Ghaddar and Prof. Fouad Azizi for their guidance and constructive comments.

Last but not least, I would like to convey my deepest gratitude to my friends and family who kept me motivated during my research.

ABSTRACT

OF THE THESIS OF

Jamil Fadi El Masry

for

Master of Science

Major: Energy Studies

Title: Assessing the Role of PCM and Well Design in Enhancing the Performance of Coaxial Geothermal Wells

Geothermal energy is becoming a promising source of clean energy as the world transitions away from fossil fuels. It can be exploited through a closed loop system where a fluid circulates from the surface to underground formations in a closed well and exits at higher temperatures. Major problems in closed loop geothermal wells include the early thermal depletion of the formation around the well, and thermal short circuiting due to the long distance travelled by the fluid back to the surface. Conventional ways to reduce the impact of such problems is to install an insulation around the tubing and regulate the operation conditions of the well to optimize heat extraction and formation thermal depletion.

In this work, a two-dimensional axisymmetric coaxial geothermal well model of depth 1000 m is simulated by coupling fluid flow and heat transfer using the finite element method. The simulated well model is benchmarked and validated against a steady state model. The thermal energy production is studied for different well design by varying the inner pipe thickness, the properties of the grout, and including an air gap or phase change material to the inner pipe.

The results displayed improvement in the well performance after increasing the inner pipe thickness from 1 cm to 2 cm and using thermally enhanced grout by 65% and 3.6%, respectively. Moreover, geothermal well performance improved after the deployment of an air gap inside the inner pipe with an optimal performance improvement of 5.54% achieved for an air gap height of 400 m. Furthermore, adding PCM in the inner pipe shows enhancement in the overall well performance. Finally, the analyses were complemented by an economic evaluation by calculating the levelized cost of energy for each model. Models with an inner pipe gap have the lowest LCOE among the studied models.

TABLE OF CONTENTS

ACKNOWLEDGEMENTS	1
ABSTRACT.....	2
ILLUSTRATIONS.....	5
TABLES.....	7
ABBREVIATIONS	8
INTRODUCTION	10
1.1. Objectives	13
LITERATURE REVIEW.....	15
2.1. Coaxial Heat Exchangers.....	15
2.2. Geothermal Wells Backfill Materials (Grout)	17
2.3. Parameters Affecting the Geothermal Well Performance	19
2.4. Phase Change Materials.....	27
2.5. Review on the Incorporation of PCM in Geothermal Applications	29
METHODOLOGY.....	33
3.1. Model Description	33
3.2. Mathematical and Numerical Approach	36
3.2.1 Heat Transfer and Phase Change Equations	36
3.2.2. Fluid Flow Model Equations	39

3.2.2 Numerical Approach.....	41
3.3. Model Domain Materials and Properties	42
3.4. Initial and Boundary Conditions.....	44
3.5. Modeling Scenarios	46
3.5.1. Scenario 1: Base Model	46
3.5.2. Scenario 2: Model with Grout	46
3.5.3. Scenario 3: Model with Inner Pipe Air Gap	46
3.5.4. Scenario 4: Model with Inner Pipe PCM Gap	46
3.6. Performance and Economic Evaluation Methodology	47
3.7. Assumptions and Limitations	49
RESULTS AND DISCUSSION	50
4.1. Model Benchmark.....	50
4.2. Results.....	52
4.2.1. Scenario 1: Inner Pipe Thickness Analysis.....	52
4.2.2. Scenario 2: Grout Material Analysis	54
4.2.3. Scenario 3: Inner Pipe Air Gap Analysis	56
4.1.4. Scenario 4: Inner Pipe PCM Gap Analysis.....	63
4.3. Performance Evaluation of Simulated Models	66
4.4. Economic Analysis of the Models	70
4.5. Future Research Suggestions	75
CONCLUSION	76
APPENDIX A	77
REFERENCES.....	79

ILLUSTRATIONS

Figure

1. Configuration of (A) Coaxial DHE and (B) U-Tube DHE retrieved from Kurnia et al., 2021 [1]	12
2. Schematic representation of coaxial heat exchanger, retrieved from Budiono et al. [3]	16
3. Structure diagram showing the modes of heat transfer in a coaxial heat exchanger system retrieved from Zhang et al. [11]	17
4. Common types of grout materials in geothermal energy systems, retrieved from Mahmoud et al. [28].....	19
5. Classifications of phase change materials retrieved from Barbi et al. [17], Tariq et al. [30], and Mahmoud et al. [28]	28
6. Cross-section of the coaxial BHE model representing model domains.....	34
7. (a) Schematic representation of the well and formation. (b) Locations within the model where the simulation parameters (e.g., temperature) are measured. The figure is not drawn to scale.	35
8. Cross-section of the modified coaxial BHE model (not to scale).....	36
9. Phase change profile of the PCM (taken from COMSOL).....	39
10. Model initial and boundary conditions	45
11. Variation of outlet temperature with time (Point A) for models in scenario 1 ...	52
12. Variation of temperature with time in the bucket space (Point B) for models in scenario 1	53
13. Variation of temperature along the inner pipe centerline at different operation times for models in scenario 1	54
14. Variation of outlet temperature (Point A) with time for models in scenario 2 ...	55
15. Variation of temperature with time in the bucket space (Point B) for models in scenario 2	56
16. Annular centerline temperature results at t=0.5 year (left) and t=60 years (right) for models in scenario 2.....	56
17. Variation of outlet temperature (Point A) with time for models in scenario 3 ...	57
18. Variation of temperature with time in the bucket space (Point B) for models in scenario 3	57

19. Variation of temperature along the inner pipe centerline at different operation times for models in scenario 3	58
20. Radial temperature profile of the formation at formation cutline with depth $z=-999.9$ m for base model.....	59
21. Radial temperature profile of the formation at formation cutline with depth $z=-999.9$ m after 60 years for models in scenario 3	60
22. Temperature at the well-formation interface line at operation times 0.1, 15, and 60 years for models in scenario 3	61
23. Temperature at the annular centerline at operation times 0.1, 15, and 60 years for models in scenario 3	62
24. Temperature profile of the first 50 m section of the inner pipe for the base model	63
25. PCM materials offered by PlusICE manufacturer [48]	64
26. Outlet temperature results (Point A) for models in scenario 4	65
27. Phase change profile of the PCM at different depths in the gap.....	66
28. Variation of thermal energy output with time for models simulated in scenario 1	67
29. Variation of thermal energy output with time for models simulated in scenario 2	67
30. Variation of thermal energy output with time for models simulated in scenario 3	68
31. Variation of output power with time for models simulated in scenario 4	69
32. Common expenditure and risk profiles of any geothermal project [49], [50]	71

TABLES

Table

1. Factors influencing the heat transfer performance of DBHEs based on Pan et al. [26].....	20
2. Features of coaxial BHE well modeled for studies in the literature	22
3. Findings of the analyses performed on coaxial BHE well models listed in Table 2	23
4. Well model geometry specifications.....	34
5. Dimensions of the modified coaxial BHE model (* refers to a value that is study dependent).....	35
6. Materials used in each domain and their corresponding properties (COMSOL Material Library, [6], & [43])	43
7. Model benchmark results against Caulk & Tomac, 2017 [6]	51
8. Properties of the selected PCM chosen based on the inner pipe temperature profile of Figure 23 and the manufacturer (PlusICE)	64
9. Estimated overall thermal energy output of the simulated models	69
10. Costs associated with the geothermal well model	73
11. Economic evaluation of the studied models	74

ABBREVIATIONS

Latin

- C_p : Specific heat capacity at constant pressure of the material in J/Kg.K
 $C_{p,1}$: Specific heat capacity at constant pressure of the material in phase 1 in J/Kg.K
 $C_{p,2}$: Specific heat capacity at constant pressure of the material in phase 2 in J/Kg.K
 $C_{\text{drilling\&completion}}$: Drilling and completion costs of the well in \$\
 C_{grout} : Cost of the backfill material in \$\
 C_{fluid} : Cost of the working fluid which is water in this case in \$\
 C_{PCM} : Cost of PCM deployed in the gap in \$\
 $C_{\text{o\&m}}$: Operation and maintenance cost in \$\
 c_{out} : Heat capacity of the working fluid at the outlet in J/Kg.K
 c_{in} : Heat capacity of the working fluid at the inlet in J/Kg.K
 D : Characteristic diameter of the pipe/well in m
 D_g : Diameter of the grout domain in m
 D_c : Casing diameter in m
 D_o : Tubing outer diameter in m
 D_i : Tubing inner diameter in m
 D_t : Thin inner pipe diameter in m
 g : Gravitational acceleration in m/s²
 $G.G$: Geothermal gradient in °C/m
 H : Well depth in m
 H_f : Formation depth in m
 I : Identity matrix
 k : Thermal conductivity of the material in W/m.K
 L_i : Length of the inner pipe in m
 L_{air} : Length of the inner pipe air gap in m
 $L_{1\rightarrow 2}$: Latent heat capacity of the material in J/Kg
 \dot{m}_{out} : Outlet mass flowrate in Kg/s
 \dot{m}_{in} : Inlet mass flowrate in Kg/s
 p : Pressure in Bar
 p : Contact pressure in Pa
 p_{init} : Initial pressure at any point in the system in Pa
 p : Inlet pressure or pressure at the reference in Pa
 p_{hydro} : Hydrostatic pressure in Pa
 Q : Heat flux in W/m²
 Q : Thermal energy output in kWh
 q_r and q_z : Conductive heat flux vector components
 Re : Reynold's Number
 R : Formation radius or domain width in m
 r : Radial distance away from the centerline of the well in m
 r and z : Radial and axial coordinates
 T : Temperature of the material in K
 T_f : Formation Temperature in °C
 T_{surf} : Surface ambient temperature in °C
 T_{out} : Outlet temperature in K

T_{in} : Outlet temperature in K
 $T_{pc,1\rightarrow 2}$: Phase change temperature in K
 TC: Total cost in \$
 t: Time in s
 u: Fluid inlet velocity in m/s
 u_r and u_z : Velocity vector components
 W_{out} : Output power in J/s
 X: Bucket space in m
 X': Gap thickness in m
 z: Vertical height in m
 z_{ref} : Elevation of the reference in m

Greek

$\Delta T_{1\rightarrow 2}$: Phase change temperature range in K
 ρ_{ref} : Fluid density at the reference in kg/m^3
 μ : Dynamic viscosity in Pa.s or in Kg/m.s
 ρ : Density of the material in kg/m^3
 θ_1 : Fraction of phase 1
 θ_2 : Fraction of phase 2

Vector Quantities

F: Body external force vector in N/m^3
g: Gravitational acceleration vector in m/s^2
q: Conductive heat flux vector in W/m^2
u: Fluid velocity vector in m/s
 \hat{r} and \hat{z} : Unit radial and axial vectors

Abbreviations

BHE: Bottomhole heat exchanger
 CLSM: Controlled low strength material
 COP: Coefficient of Performance
 DBHE: Deep bottomhole heat exchanger
 EGS: Enhanced geothermal system
 GHE: Ground Heat Exchanger
 GSHP: Ground Source Heat Pump
 HDR: Hot dry rock
 HWR: Hot wet rock
 LCOE: Levelized cost of energy in \$/kWh
 MPCM: Microencapsulated Phase Change Material
 MPCS: Microencapsulated Phase Change Slurry
 MD: Measured depth in m
 NPs: Nanoparticles
 PCM: Phase change material
 SSPCM: Shape stabilized phase change material
 TC: Thermal Caisson

CHAPTER 1

INTRODUCTION

The continuous increase of energy demand, price volatility of oil and gas and their associated environmental footprints have all pushed towards putting more efforts to develop and exploit other cleaner and renewable energy sources [1]. Unlike other renewable sources, geothermal energy is independent of the meteorological conditions, and hence it is more viable [2], [3]. Geothermal resources are irregularly distributed and mainly fed by dissipating thermal energy from earth's core to the surface, this results in geothermal gradients ranging between 20°C/km and 150°C/km depending on the location and geologic conditions [1], [2]. Geothermal resources are classified into three main categories according to the formation's temperature: (1) high enthalpy resources of temperature greater than 180°C, (2) middle enthalpy resources of temperature ranging between 100°C and 180°C, and (3) low enthalpy resources of temperature below 100°C [4].

Geothermal energy projects are capital expensive, in order to cut the high drilling costs associated with geothermal projects, recent approaches suggest the repurposing of existing abandoned and depleted oil and gas wells [1], [5]–[8]. However, oil and gas reservoirs are usually low enthalpy resources and result in lower outlet temperatures [1]. The outlet temperature of geothermal well determines the type of powerplant to be installed [1] for example dry steam, flash steam, and binary powerplants [9], [10].

Enhanced geothermal systems are classified into open loop and closed loop systems. Open loop geothermal energy extraction involves two or more wells to extract heat (with at least 1 injection and 1 extraction wells). Working fluid (typically water) is injected through the injection well and is collected back through the extraction well after exchanging heat with the formation [1], [7]. Closed loop geothermal systems include 4 types which are borehole heat exchanger systems, ground source heat pump systems, coaxial downhole heat exchanger (DHE) systems, and U-tube downhole well systems [11]. Ground source heat pump and borehole heat exchanger systems are integrated in shallow geothermal reservoirs, while the coaxial and U-tube downhole heat exchangers are typically deployed for medium to deep geothermal resources [11]. Double pipe or coaxial downhole heat exchanger has a larger heat exchange area and higher working fluid volume to exchange heat with the formation compared to the U-tube DHE. Moreover, implementing coaxial DHE requires lower pumping power and less cement than a U-tube configuration [1], [7], [12]. The area surrounding the pipes is pumped with grout of high thermal conductivity to facilitate heat flow from the formation to the well [8]. The configuration of coaxial and U-tube downhole heat exchangers is illustrated in Figure 1.

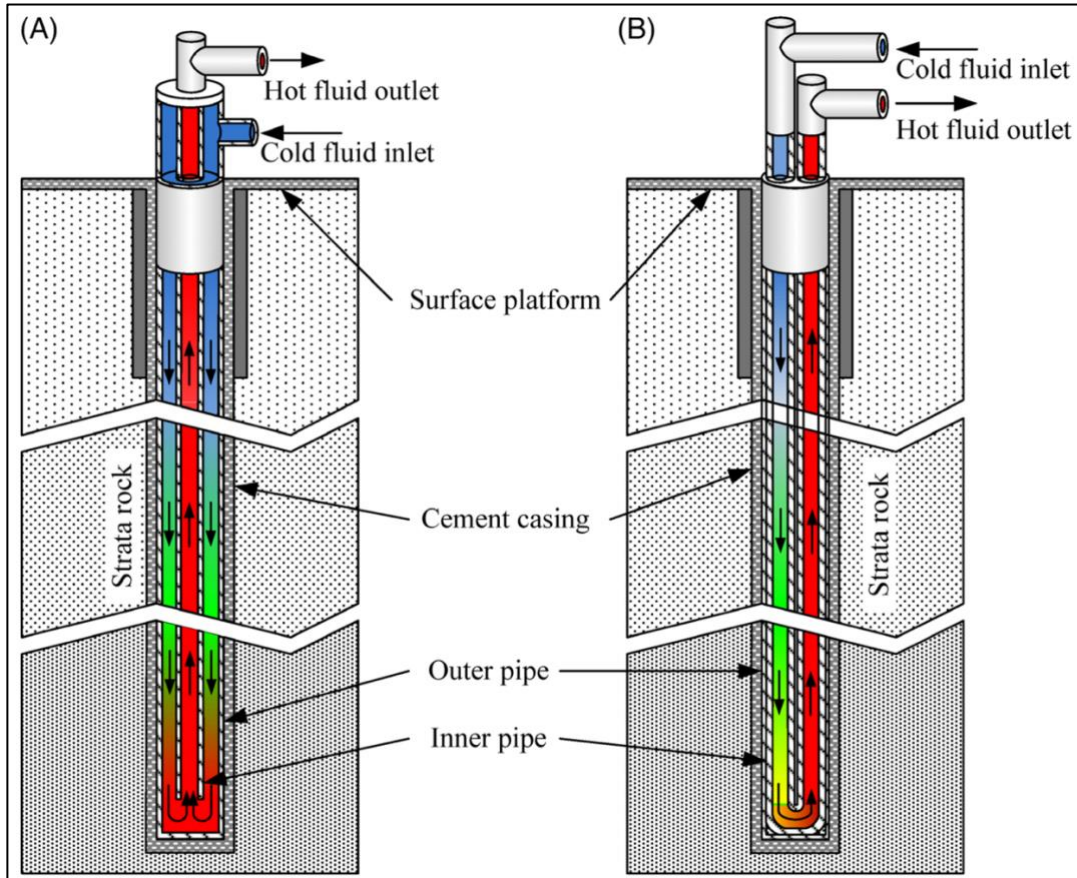


Figure 1 Configuration of (A) Coaxial DHE and (B) U-Tube DHE retrieved from Kurnia et al., 2021 [1]

Several assessments have been performed on the application of latent heat storage using phase change materials (PCM) in geothermal applications, commonly ground source heat pumps (see section 0). PCM are substances that release or store energy in the form of latent heat by changing phase and are characterized by a high thermal heat storage capacity [13], [14]. PCM are classified into 3 categories based on their phase change, PCM are either solid-solid, or solid-liquid, or liquid-gas, however, the solid-liquid PCM is the most widely used in thermal storage systems. This is mainly because they have large values of latent heat, negligible volume change, and a range of melting temperature [14]. Heat is stored by the PCM and is transferred to the working fluid when there is an excess of heating and cooling loads [13]. Utilizing PCM in geothermal projects can improve the coefficient of performance (COP) of the system

which is ratio of thermal heat extracted to the work consumed by the pump. The selection of the PCM is critical to the environment where it is installed since the melting point of the PCM (i.e, transition from solid to liquid) must be reached to store and release energy in the form of latent heat [13]. PCMs are usually integrated within the ground source heat pumps (GSHP) systems, either in the borehole or in a storage apparatus such as an external tank outside the borehole [15], [16]. PCM significantly improves the short-term COP of the GSHP system, however, long term improvement is lower [13].

Although the performance of integrating PCM in shallow (maximum depth of 400 m) borehole heat exchanger and ground source heat pump systems in building applications has been studied and understood [13]–[19], the performance of PCM in medium to deep depths (600 m-3000 m, [20]) downhole heat exchangers such as repurposed abandoned oil and gas wells is yet to be investigated and discussed. The performance of incorporating PCM in deep geothermal wells for short- and long-term applications is still nebulous and missing from the literature. Therefore, the focus of the thesis is to investigate the feasibility of incorporating PCM and the effect of other well design parameters on geothermal energy performance.

1.1. Objectives

The main objectives of this research are summarized as follows:

- 1) Study the influence of well design parameters on the performance of coaxial geothermal well including the inner pipe thickness, the grout thermal properties, and the addition of an air gap inside the inner pipe.

- 2) Assess the performance of adding PCM in a gap of the inner pipe compared to an air gap and the methodology for PCM selection.
- 3) Study the economic feasibility of these solutions to enhance geothermal well performance.

CHAPTER 2

LITERATURE REVIEW

In this section, an overview of the literature on coaxial geothermal wells, their configuration, heat transfer profile, and grout material is illustrated along with the reported studies on the well parameters affecting their performance. Moreover, phase change materials are discussed with a review on their implementation in geothermal energy applications.

2.1. Coaxial Heat Exchangers

A coaxial closed loop heat exchanger is composed of two concentric pipes as shown in Figure 2. The working fluid (heat carrier) is injected through the annular space, which is the space between the casing and the inner pipe. and is produced through the insulated inner pipe (tubing) this is referred to as reverse circulation [3], [7], [11], [21]. The schematic of a coaxial closed loop heat exchanger is illustrated in Figure 2.

Injected cold working fluid (typically water) is heated by the formation while descending in the annulus, the fluid reaches the bottom of the well and returns to the surface through the insulated tubing [21]. However, the heat loss from the hot produced fluid in the inner pipe to the cold injected fluid in the annulus reduces the efficiency of the system [11], [12], [21]. Consequently, the inner pipe material must have high thermal resistance, which means either high thickness or low thermal conductivity.

Typical inner pipe materials used include polypropylene, polyethylene, or polyvinyl chloride (PVC) [12], [22].

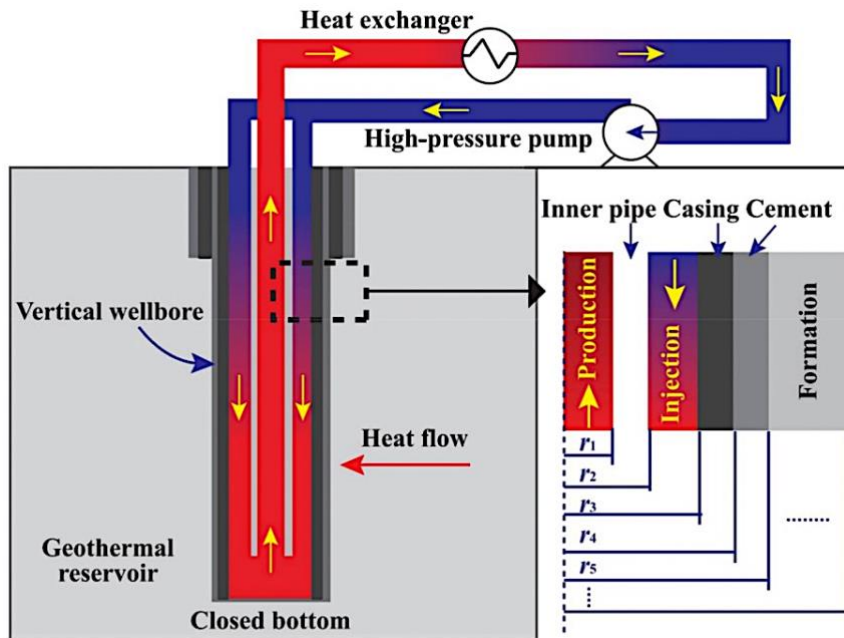


Figure 2 Schematic representation of coaxial heat exchanger, retrieved from Budiono et al. [3]

The following modes of heat transfer are dominant in each section of a coaxial geothermal well model [3], [7], [11], [12], [21]:

- Geothermal Reservoir: Heat conduction is the main mode of heat transfer in the geothermal reservoir. The presence of an aquifer or a high permeability formation (i.e., fluid flow) promotes heat convection.
- Grout and Casing: Heat transfer from the formation to the working fluid occurs by conduction through the grout and the casing.
- Working fluid: The flowing fluid collects heat from the casing inner walls and the outer walls of the inner pipe through forced convection, natural convection occurs within the working fluid domain due to vertical temperature differences.

- Inner pipe and insulation: Heat transfer mode is conduction through the inner pipe that can include a plastic tubing, foam insulation, vacuum/air gap, or insulation fluid gap.

The modes of heat transfer in the domains of a coaxial heat exchanger model are demonstrated in Figure 3.

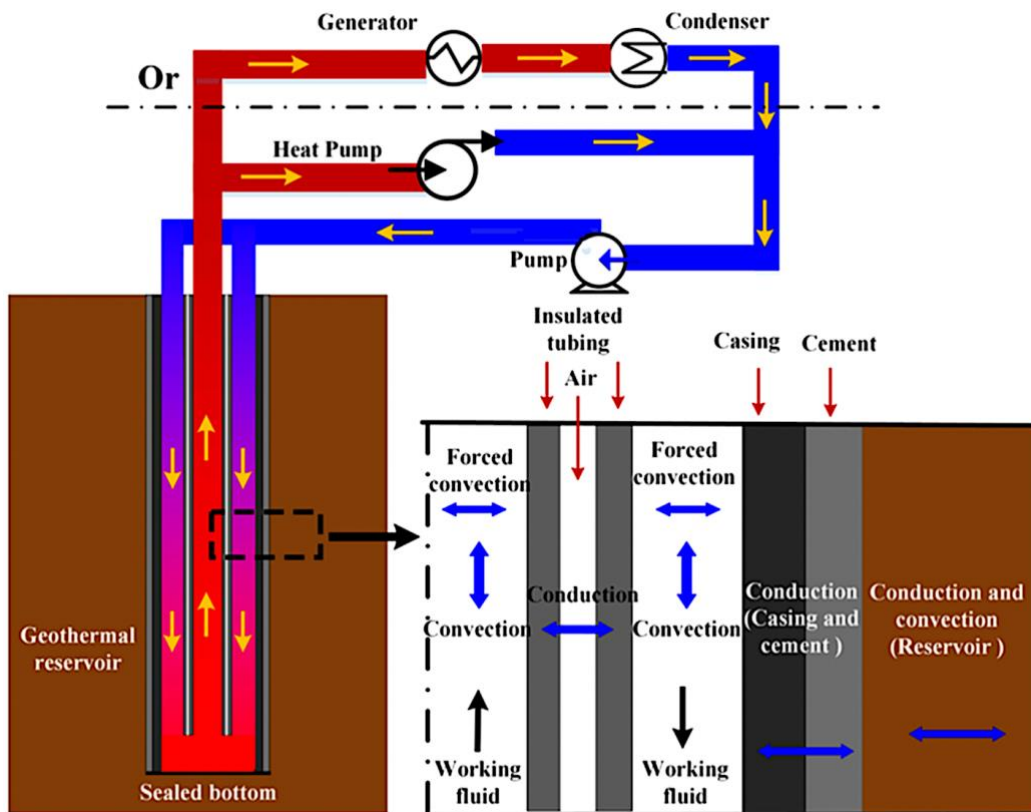


Figure 3 Structure diagram showing the modes of heat transfer in a coaxial heat exchanger system retrieved from Zhang et al. [11]

2.2. Geothermal Wells Backfill Materials (Grout)

After drilling a geothermal well and placing the casing, the well is cemented to ensure zonal isolation between the well and the formation (and ensure wellbore stability). The cement (grout) may promote the heat transfer between the formation and the BHE to achieve desired thermal performance [23], [24]. The grout must meet

several requirements for better well performance. For example, the thermal conductivity must be equal to that of the surrounding formation [23], [24]. Moreover, void spaces in grouts and between the outer coaxial pipe and the formation must be minimized in order to improve thermal interference and heat transfer which means that a grout material should not have high shrinkage [24], [25]. Grout must be thoroughly filled in the gap between the formation and the borehole in order to ensure that aquifers and formation chemicals do not get in contact with the well and avoid leakages and contamination [24]. The smaller the size of the grout's particles, the higher the heat capacity of the material. Common grout sizes include clay, silt, and coarse sized particles. Constructed BHE length is related by the properties of the selected grout material, for instance; higher grout conductivity decreases the required length of the constructed BHE [23]. Grout materials utilized in geothermal applications are classified into 4 categories, these include conventional grout materials, additives, modern grout materials and drilling cuttings as represented in Figure 4 [23], [25].

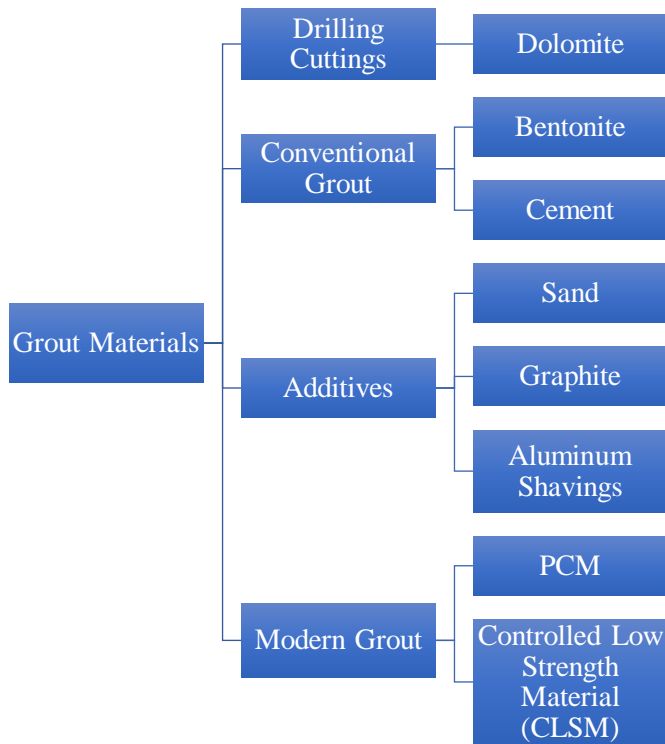


Figure 4 Common types of grout materials in geothermal energy systems, retrieved from Mahmoud et al. [28]

2.3. Parameters Affecting the Geothermal Well Performance

The depth of a deep bottom hole heat exchangers (DBHEs) may reach depths beyond 3 km to intersect the thermal reservoir. Recent studies showed that the geothermal gradient and the formation's thermal conductivity are the main factors that affect the thermal recovery from DBHEs [5]. Table 1 describes the main factors that affect the performance of a DBHE. The first column indicates the parameter and the second column indicate if the *increase* of that parameter enhances the performance of the well ('positive') or hinders it ('negative'), or whether the performance is critical to the material.

Table 1 Factors influencing the heat transfer performance of DBHEs based on Pan et al. [26]

Parameter	Influence on DBHE Performance
Residence time of the working fluid (flowrate)	Positive
Borehole diameter	Positive
Outer pipe diameter	Positive
Outer pipe thermal conductivity	Positive
Inner pipe diameter	Negative
Inner pipe wall thermal conductivity	Negative
BHE depth	Positive
The type of the pipe material	Depends on the material
Type of grout material	Depends on the material
Grout material thermal conductivity	Positive

Closed loop geothermal wells have many advantages over open loop ones, these include independence on the geothermal reservoir permeability, reducing the risk of inducing seismicity, and less environmental side effects due to the absence of contact between the working fluids and the reservoir rock [3]. Several recent studies have focused on the performance of closed loop geothermal wells. These include retrofitting abandoned oil and gas wells, assessing the performance of field applied closed loop geothermal wells, assessing the performance of well designs and reservoir properties, and on the modalities of heat transfer between the reservoir and the well [3], [27]. In closed loop geothermal wells, coaxial model has a wide range of advantages over the U-tube model, due to higher heat exchange area and higher working fluid volume, less pumping power, higher recovered thermal power, and less amount of deployed grout [1], [7], [12]. Fluid circulation in a coaxial BHE is either forward or reversed circulation. Forward circulation is when the working fluid is injected through the inner central pipe and produced through the annulus, whereas in reversed fluid circulation the working fluid is injected through the annulus and produced from the central pipe [11], [28]. Case studies performed by Zhang et al. [11] and Morita et al. [28] have shown that reverse fluid circulation generates higher thermal output. In this section, a brief

literature of recent numerical simulations performed on coaxial closed loop geothermal systems is illustrated. The features of the simulated well model of each study is represented in Table 2.

Table 2 Features of coaxial BHE well modeled for studies in the literature

<i>Reference</i>	<i>Well Depth (m)</i>	<i>Casing Inner Diameter (mm)</i>	<i>Casing Outer Diameter (mm)</i>	<i>Inner Pipe Outer Diameter (mm)</i>	<i>Inner Pipe Inner Diameter (mm)</i>	<i>Domain Size and Shape (m)</i>	<i>Software</i>	<i>Circulation Mode</i>
[29]	500	161.7	177.8	114.3	103.88	100 m x 100 m x 600 m rectangular prism	ANSYS	Reverse circulation
[21]	3500	177.8	197.8	96.2	76.2	140 m radius cylinder with 200 m extent of the reservoir beneath the well	COMSOL	Reverse circulation
[30]	2500	203.2	219.56	140.1	127	-	COMSOL	Reverse circulation
[11]	1800	230.4	269.9	114.3	62	40 m radius cylinder	MATLAB & COMSOL	Reverse circulation
[31]	3300	340	350	185	150	1000 m x 1000 m x 1000 m cube	COMSOL	Reverse circulation
[32]	1600	-	180	120	-	200 m radius cylinder	COMSOL	Reverse circulation
[33]	5000	212.8	235	114	100.6	1000 m x 1000 m rectangular prism	FEFLOW	Reverse circulation
[7]	-	150	196	80	40	40 m radius cylinder	FlexPDE	Reverse circulation
[34]	5593	228.6	244.475	101.6	76.2	-	-	Reverse circulation

The variables assessed, parameters varied, and the findings of the studies listed in Table 2 are tabulated in Table 3.

Table 3 Findings of the analyses performed on coaxial BHE well models listed in Table 2

<i>Reference</i>	<i>Studied Variables</i>	<i>Sensitivity Variable Parameters</i>	<i>Reported Findings</i>
[29]	<ul style="list-style-type: none"> • Outlet temperature • Power generated • Pressure loss 	<ul style="list-style-type: none"> • Time • Volumetric flowrate • Inlet temperature • Formation thermal conductivity 	<ul style="list-style-type: none"> • The numerical and experimental results of the generated power and the outlet temperature are comparable. • Outlet temperature drops with time and with increasing the volumetric flowrate and increases with increasing the fluid's inlet temperature. • Thermal power drops gradually with time and higher volumetric flowrate yields higher thermal power. • Increasing the fluid's inlet temperature lowers the total extracted energy and the average thermal power. • Outlet temperature, thermal power, total extracted energy, and the average power increase with the thermal conductivity of the formation.
[21]	<ul style="list-style-type: none"> • Outlet temperature • Well and formation temperature profile • Geothermal well power 	<ul style="list-style-type: none"> • Domain radius • Depth • Time • Mass flowrate • Inlet temperature • Thermal conductivity of insulated inner pipe • Insulation length of well casing 	<ul style="list-style-type: none"> • Outlet temperature at 25 years remained constant for a domain radius higher than 80 m, hence it is the maximum influence range for such operation time. • The temperature of the formation at 25 years slightly increases near the well at depths shallower than 500 m making a down-concave temperature isosurfaces while up-concave temperature isosurfaces at deeper depths. • Output temperature and the geothermal power significantly drop during the first 5 years. • For t=25years, the outlet temperature drops linearly with increasing the mass flowrate. Geothermal well power on the other hand increases logarithmically with injection rates. • Outlet temperature and geothermal power is linearly dependent on the inlet temperature, where the outlet temperature increases with the inlet temperature unlike geothermal power and inner pipe thermal conductivity inner pipe thermal conductivity that decreases. • Outlet temperature and geothermal well power drop linearly with inner pipe thermal conductivity.
[30]	<ul style="list-style-type: none"> • Well temperature profile • Net power output 	<ul style="list-style-type: none"> • Tubing diameter • Insulation thickness • Mass flowrate • Geothermal gradient 	<ul style="list-style-type: none"> • Outlet temperature increased with insulation thickness. • Turbine net work output increases with the geothermal gradient and depth. • Net power output increases with the fluid flowrate to a certain limit for all tubing diameter cases, smaller tubing diameters require less flowrate to minimize pressure drop in the tubing.

	<ul style="list-style-type: none"> • Thermal efficiency 	<ul style="list-style-type: none"> • Type of working fluid • Well depth 	<ul style="list-style-type: none"> • Thermal efficiency increases with the geothermal gradient, however; it decreases with higher flowrates under constant geothermal gradient for all tested working fluids. • Refrigerants can operate at higher flowrates than hydrocarbons and hence yield higher net work output. • The optimal well design which yielded a shorter payback period of 2.25 years, 20.89 GWh/year, and an LCOE of 0.46 \$/KWh. is the one with a tubing diameter of 0.127 m and 2500 m depth.
[11]	<ul style="list-style-type: none"> • Well temperature profile • Outlet temperature • Thermal power • Coefficient of performance (COP) • Pressure loss 	<ul style="list-style-type: none"> • Time • Inlet temperature • Volumetric flowrate • Formation thermal conductivity, porosity, and permeability • Working fluid type, thermal conductivity, density, and viscosity • Fluid heat capacity at constant pressure (C_p) and heat capacity ratio (C_p/C_v) • Tubing diameter 	<ul style="list-style-type: none"> • Thermal perturbation in the formation reached a radial distance of 10 m after 120 days of operation time indicating that the chosen domain radius is reasonable. • Bottomhole temperature drops sharply within few days of production period, however; the recovery period took 60 days for the formation to nearly restore its initial temperature. • Well production and recovery reached equilibrium within one year of operation time. • Both the outlet temperature and thermal power for all studied working fluids dropped sharply within the first 7 days of operation time before becoming gradually stable. • Among the tested working fluids, R600a yielded the highest output temperature while CO₂ generated the highest thermal power after 120 days of operation, water showed the least output temperature. • Thermal power of all working fluids decreases with inlet temperature and tubing diameter. • CO₂ displayed the best performance, however; water and R152a showed good performance in terms of pressure losses and integration with ORC. • Increasing the volumetric flowrate reduces the outlet temperature of all studied working fluid. • CO₂ is more sensitive to the reservoir parameters than other fluids. • Increasing rock's thermal conductivity improves the well's thermal performance unlike reservoir porosity, • Among the fluid parameters, density has the greatest influence on the thermal power, whereas both the fluid's thermal capacity and density dropped the outlet temperature with their increase.
[31]	<ul style="list-style-type: none"> • Well temperature profile • Outlet temperature • Pressure and pressure loss • Heat capacity • Thermal power 	<ul style="list-style-type: none"> • Time • Insulation length • Central tubing and annulus dimensions 	<ul style="list-style-type: none"> • Annular bottomhole temperature dropped rapidly at the beginning of production then it remained constant for 24 years before noticeable drop occurred. • Annular bottomhole pressure increased rapidly due to CO₂ accumulation at the injection wells inlet. • Wellhead and bottomhole temperatures decreased gradually with time till year 24 where noticeable drop is observed. • Heat flowrate between the formation and the annulus at the beginning of production was high due to high temperature difference, then it dropped to a constant value. • Increasing the insulation length of the tubing significantly improved the tubing wellhead temperature while reduced annular bottomhole temperature. • Increasing the annulus and tubing size increased bottomhole and wellhead temperatures.

<p>[32]</p> <ul style="list-style-type: none"> • Outlet temperature • Coefficient of performance (COP) 	<ul style="list-style-type: none"> • Well depth • Fluid mass flowrate • Geothermal gradient 	<ul style="list-style-type: none"> • Increasing annular space has no influence on the well's temperature and annular wellhead pressure. • The optimal flowrate in the analysis (1 l/s) is necessary to achieve a temperature increase >10°C for 1000 m deep well. • Increasing the geothermal gradient increases the outlet temperature for all depths and fluid flowrate cases. • Fluid flowrate and geothermal gradient become more impactful on the outlet temperature with depth. • COP drops with higher fluid flowrates and increases with well depth. • For high flowrates (>1 l/s) the COP increases almost linearly with depth, while for smaller flowrates the COP increases with depth until it peaks before starting to drop at depths >3000 m.
<p>[33]</p> <ul style="list-style-type: none"> • Outlet temperature 	<ul style="list-style-type: none"> • Groundwater flux • Thermal conductivity of the formation, grout and the inner pipe. • Volumetric flowrate • Time • Inlet temperature • Geothermal gradient • Volumetric heat capacity of the formation • Reservoir porosity • Subsurface thermal dispersivity 	<ul style="list-style-type: none"> • Thermal performance of BHE is improved with groundwater flux and thermal conductivity of the grout and the formation. • Loop outlet temperature got slightly affected by varying the formation's volumetric heat capacity. • Porosity has negative impacts on the outlet temperature where higher porosity slows thermal recovery. • Geothermal gradient had a great influence on thermal recovery, where vertical distribution of formation temperature significantly affected the loop outlet temperature. Gained temperature increased from 3.7 °C to 7°C at 25 years corresponding to 0.02 and 0.05 K/m geothermal gradients respectively. • Reducing the thermal conductivity of the inner pipe from 45 to 1W/m.K significantly enhanced the loop outlet temperature from 4.8°C to 13.9°C. • Reducing inlet temperature from 5 to -5°C slightly influenced the thermal plume extent and the grout temperature at 5000 m depth, while it increased temperature gain from 4.1 to 5.5°C at 25 years. • Increasing the fluid's volumetric flowrate extended the thermal plume in the formation, dropping the flowrate from 300 to 150 m³/day increased the outlet temperature from 4.8 to 5.7°C. Higher flowrates of 450 and 600 m³/day had slight effects on the outlet temperature after 25 years.
<p>[7]</p> <ul style="list-style-type: none"> • Outlet temperature • Inlet temperature • Steady state power 	<ul style="list-style-type: none"> • Inlet temperature • Geothermal gradient • Time • Reservoir thermal conductivity • Mass flowrate • Groundwater flow 	<ul style="list-style-type: none"> • Casing insulation at depth where formation temperature = fluid inlet temperature increased the outlet temperature by 4.4°C. • Increasing the inlet temperature increased the outlet temperature while decreased the stationary power. • Steady state power increases with fluid flowrate until it reaches a plateau. • Heat exchanger performance improved with reservoir thermal conductivity and geothermal gradient. • Higher downward groundwater flow diminishes the performance of the heat exchanger. • For a constant output power over 15 years of operation time, fluid inlet temperature must gradually decrease w.r.t outlet temperature (i.e., constant temperature difference). • Influence of mass flowrate on output power is less than that of the outlet-inlet temperature difference.

[34]

- Outlet temperature
- Ideal work production rate
- Carnot engine work rate
- Time
- Volumetric flowrate
- Well diameter
- Casing length
- Insulation thickness
- Tubing diameter
- Volumetric heat capacity
- Basal heat flux
- Formation thermal conductivity and thermal volumetric heat capacity
- Outlet temperature and the ideal work rate drop rapidly at the beginning of production until it enters into a pseudo-steady state (state where drop is linear) at day 500.
- Reducing the flowrate by five times increased the outlet temperature at PSS, however; increasing this value by five times dropped the outlet temperature at PSS from 84 to 40 °C.
- Ideal work is dependent on the flowrate and the outlet temperature.
- Doubling the well diameter increased the outlet temperature by 11°C and the ideal work by 50kW.
- Increasing the casing length in the open hole well and insulation around the inner tube proved to have no major influence on the outlet temperature.
- Increasing the tubing diameter affected the initial short transient period of the outlet temperature, beyond which no major influence was observed.
- Outlet temperature is unaffected by the change of the fluid thermal properties with temperature.
- Heat extraction is governed by the volumetric heat capacity.
- Outlet temperature and the ideal work extraction rate at PSS drop with the increase in basal heat flux.
- Outlet temperature at PSS is the highest in the cases where the formation's thermal conductivity and thermal volumetric heat capacity are highest.

2.4. Phase Change Materials

Phase change materials (PCM) are used for thermal energy storage purposes, such materials store latent heat of 5-14 times more than sensible heat for the same volume [17]. They are mainly characterized by large heat capacity compared to other materials; however, their low thermal conductivity is a major drawback, which is circumvented by incorporating additives [14], [25], [35]. PCM in geothermal applications can avoid thermal imbalance resulting from fluctuations in cooling and heating loads keeping the temperature of the working fluid in a designed range, moreover; utilizing PCM in grout materials reduce the temperature variations in the surrounding formation [25]. Latent heat is absorbed or released when the PCM phase changes between solid and liquid. Impure PCMs undergo phase change over a given temperature range, however; pure PCM have more specified phase change temperatures (i.e., the temperature range is small) [36]. Phase change materials are either inorganics, organics, and eutectics. Organic phase change materials are paraffin or non-paraffin based, inorganic PCM include metallics and salt hydrates, and eutectic PCM are PCM mixtures [17], [23], [35]. The detailed PCM classifications are demonstrated in Figure 5.

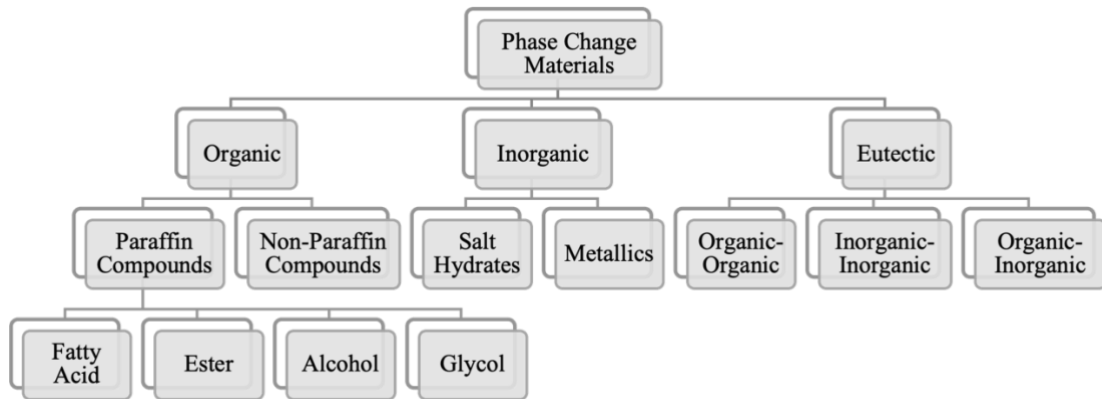


Figure 5 Classifications of phase change materials retrieved from Barbi et al. [17], Tariq et al. [30], and Mahmoud et al. [28]

Paraffin wax organic PCM is most commonly added to grout, such PCM have melting temperatures between 20°C and 70°C, fatty acid PCM have melting temperatures between 17°C and 64°C [17]. Salt hydrates are the most used inorganic PCM, these have a wider range of melting temperatures which can exceed 250°C [17]. Eutectic PCM have a sharper melting temperature than their pure constituents. Organic PCM is most integrated in the building sector due to suitable melting temperature ranges unlike inorganic PCM [17]. The application of PCM has been widely spreading recently due to their several benefits compared to other materials especially their thermal stability and thermal capacity [23]. Organic PCM are characterized by chemical and thermal stability, non-corrosiveness, and low undercooling unlike inorganic PCMs which encounter phase separation, undercooling, lack of thermal stability, and corrosion. Inorganic PCM have higher density and higher phase change enthalpy compared to organic PCM, a major disadvantage in organic PCM is their flammability and low thermal conductivity. There are limited studies on eutectic PCM, however; their sharp melting point offer desirable performance [17].

2.5. Review on the Incorporation of PCM in Geothermal Applications

PCMs commonly used in building application for thermal energy storage (TES) especially in walls have been proposed for integration in geothermal wells. In a geothermal well, PCMs are incorporated through the working fluid in the form of microencapsulated phase change slurry, or in grouts by micro/macro encapsulation, shape stabilization, or direct incorporation [17].

Soni et al. [37] investigated the stability of microencapsulated PCM (MPCM) in working fluids, MPCs with 30 wt.% MPCM at 80°C can store 30% more energy than water at the same temperature and displayed robustness, physical and chemical stability. Taherian et al. [19] investigated the heat transfer and fluid flow performance of MPCs in turbulent flow. Resulted pressure drop in MPCs under turbulent flow is close to that of water regardless of the higher viscosity of the slurry. The slurry's effective heat capacity remained intact; this proves the MPCs durable. However, the heat transfer coefficient of the slurry decreases beyond the optimal MPCM concentration and with lower flowrates. Moreover, the type of the used PCM has no effect on the heat transfer coefficient of the MPCs assuming same latent heat of fusion and mass fraction of the used PCMs. Kong et al. [38] found that more heat is transported by MPCs than water at constant pumping power and the COP of the system increased by 4.9%. Furthermore, using progressive cavity pumps helped reserving the MPCs robustness and durability after 10.5 years of operation time. Pu et al. [18] compared the performance of MPCs to water and the y shaped GHE structure to the horizontal structure. Integrating MPCs in a Y-shaped GHE structure yielded an effective enhancement in the thermal performance and a reduction in pressure losses. This combination improved the performance by 38.9% compared to water-horizontal tube system.

The integration of PCMs in geothermal grouts has a great potential to improve the thermal performance of the geothermal system through latent heat storage. Mahmoud et al. [23] reviewed several types of geothermal grout materials and compared their properties. The findings of this review show that PCMs are potential candidates for geothermal grouting due to their high heat storage capacity, temperature balance, and stability. However, PCMs are characterized by low thermal conductivity, this problem can be overcome by using composite PCMs (mixing additives or nanoparticles (NPs) to improve their properties). The incorporation of NPs in PCM enhances the thermal conductivity of the material. The preparation techniques and the applications of nano enhanced PCM are reviewed by Tariq et al. [35]. Javadi et al. [39] investigated the thermal performance of U-tube BHE by utilizing nano-enhanced PCM around the U-tube. They evaluated the performance of seven different nanoparticles with paraffin PCM in terms of NPs different volume fractions and shapes. Results have shown that 20% volume fraction of blade shaped Cu mixed with paraffin PCM yielded the best performance, it improved the thermal conductivity of the grout by 55% compared to pure paraffin PCM. However, SiO₂ NPs mixed with paraffin PCM resulted in the worst performance. Li et al. [40] studied the heat transfer performance in a single U-tube heat exchanger when utilizing shape stabilized PCM (SSPCM) as a backfill material. The SSPCM used is a mixture of decanoic and lauric acid with 6% expanded graphite, 10% silica, and 60% decanoic acid. Simulation on FLUENT software showed that heat exchange using the SSPCM backfill is 1.23 more than that when using crushed stone concrete as a backfill. Consequently, the thermal influence radius of SSPCM backfill is 90% as that of crushed stone concrete backfill. Mousa et al. [14] experimented the effect of PCM on the energy storage capacity and the thermal radius

of energy piles through implementing PCM containers into the concrete shell of the GHE. Results showed that energy storage increased from 16.4 to 48.2 kJ/kg. Eslami-nejad & Michel [15] proposed a new GHE configuration integrated with PCM, this study aims to reduce the GHE length by using PCM. It consists of a U-tube GHE with a thermally enhanced PCM ring surrounding the tube. Annual simulations on the proposed borehole configuration were performed by Eslami-nejad & Michel [15] showed that the GHE length can be hence reduced by 9%. Aljabr et al. [36] discussed the effect of adding MPCM to the grout of the GCHP, findings of their study suggested that wrong selection of the PCM by thermal properties and melting point would deteriorate the performance of the system rather than enhancing it. Moreover, the thermal conductivity of the PCM must be close to that of the grout for optimal performance. In addition, the optimal melting point of the PCM is the point at which almost all PCM in the capsules are at liquid state during the peak load. Furthermore, this study found that the utilization of paraffin MPCM in the grout can reduce the required BHE length by 7%, however; this reduction in length will not reduce the cost of the project since the money saved from drilling would be spent for purchasing PCM which is relatively expensive. Alavy et al. [13] introduced a novel thermal caisson (TC) concept (include structural components supporting the building and energy system components providing the building with heating and cooling). This concept includes GHE integrated with PCM. They specified the criteria for the selection of an optimal PCM, where an effective PCM must melt during high temperature output and solidify when the temperature output is insufficient. PCM with low thermal conductivity is ineffective since heat accumulates in the borehole rather than in the PCM, this reduces the system's performance, hence the higher the thermal conductivity of the PCM grout

the better the performance will be [13]. The conclusion of the study was that TC with incorporated PCM can reduce the capital cost by 49% (shorter payback period) and improve the stability and the coefficient of performance (COP) of the system by 16% compared to the utilization of conventional fossil fuel-based HVAC system in buildings. Chen et al. [16] examined the influence of utilizing PCM on the efficiency of the GSHP. They found that implementing PCM of low thermal conductivity in the grout would reduce the efficiency of the system. In contrary, when the PCM's thermal conductivity is close to that of the ordinary grout, the efficiency and the stability of the system are significantly improved, similarly when the formation's thermal conductivity and Darcy velocity are high. The authors also found that it is more favorable to use PCM of high thermal conductivity in the locations where groundwater is absent (Heat transfer by conduction is dominant) [16].

CHAPTER 3

METHODOLOGY

In this section, the numerical model including model description, the governed heat transfer and fluid flow equations, the sensitivity analyses, performance, and economic analyses are illustrated.

3.1. Model Description

A 2D axisymmetric coaxial BHE is modeled using finite element on COMSOL Multiphysics. The properties of the model and the boundary conditions are symmetric around the well central axis. The domains and dimensions of the proposed well model are listed in **Error! Not a valid bookmark self-reference.** and shown in Figure 6 and Figure 7. The simulated well model is benchmarked and validated against the steady state model developed by Caulk & Tomac, 2017 [6] and yields a maximum error of 5%. Moreover, a convergence study is performed to determine the optimal formation width which provides enough buffer between the well and the boundary conditions. The optimal domain width was found to be 200 m which is equal to the width suggested by Caulk & Tomac, 2017 [6].

Table 4 Well model geometry specifications

Dimension	Abbreviation	Value
Well (Casing) depth	H	1000 m
Inner pipe depth	L_i	999.8 m
Domain width	R	200 m
Formation depth	H_f	1200 m
Casing diameter	D_c	0.18 m
Bucket space thickness	X	0.2 m
Inner pipe diameter	D_t	0.12 m

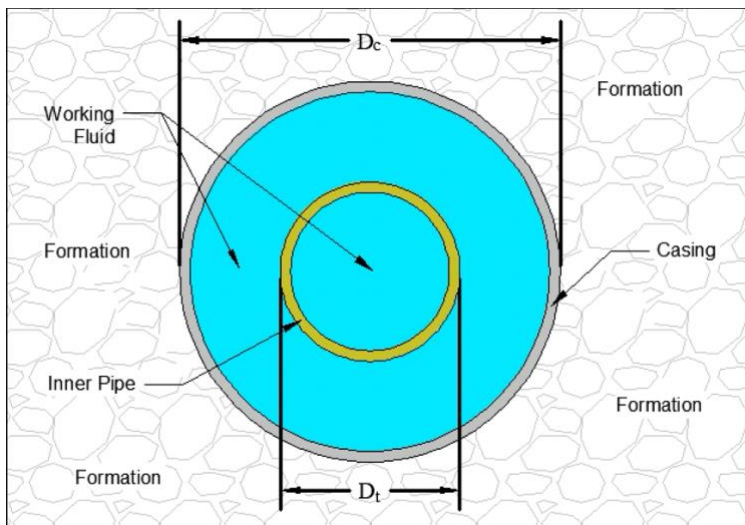


Figure 6 Cross-section of the coaxial BHE model representing model domains

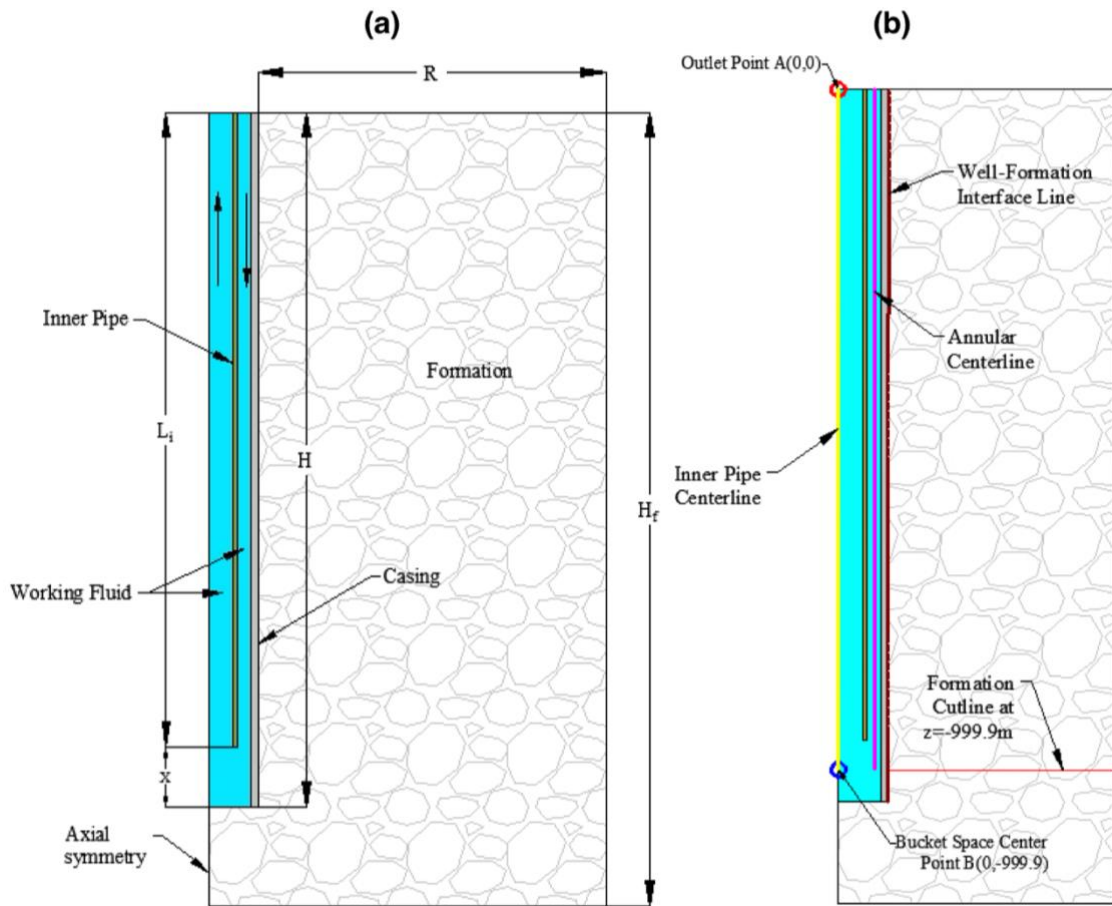


Figure 7 (a) Schematic representation of the well and formation. (b) Locations within the model where the simulation parameters (e.g., temperature) are measured. The figure is not drawn to scale.

The objective of the thesis is to study the influence of the inner pipe thickness, the presence of an air gap and PCM gap in the inner pipe, and the effect of thermal properties of the grout on the well performance. Hence, the well design parameters are modified accordingly and described in Table 5 and illustrated in Figure 8.

Table 5 Dimensions of the modified coaxial BHE model (* refers to a value that is study dependent)

Dimension	Abbreviation	Value
Casing diameter	D_c	0.18 m
Inner pipe inner diameter	D_i	[0.09-0.1-0.12] *
Inner pipe outer diameter	D_o	[0.12-0.13] *
Inner pipe air gap length	L_{air}	[200-400-999.75] *
Gap thickness	X'	1 cm
Diameter of the grout domain	D_g	0.24 m

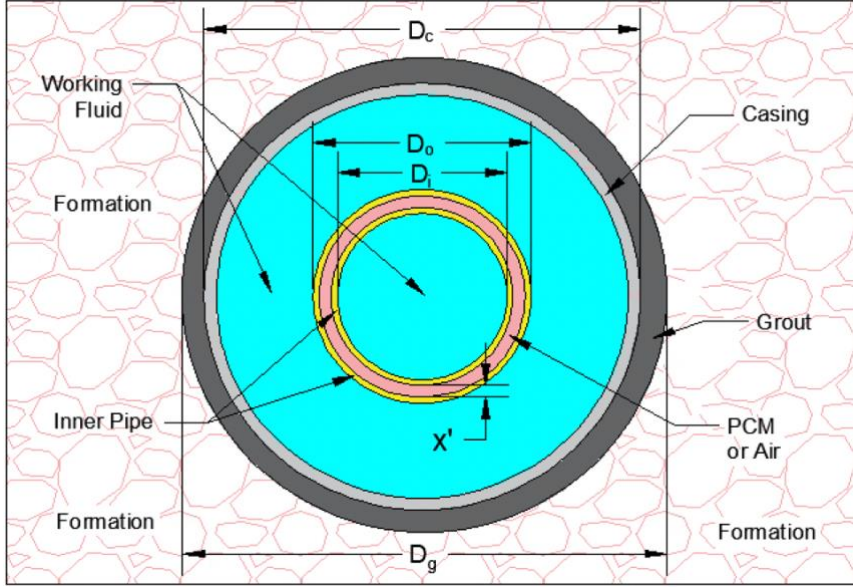


Figure 8 Cross-section of the modified coaxial BHE model (not to scale)

3.2. Mathematical and Numerical Approach

3.2.1 Heat Transfer and Phase Change Equations

The general heat transfer equation that governs heat transfer phenomenon in the simulated model is written as:

$$\rho C_p \frac{\partial T}{\partial t} + \rho C_p \mathbf{u} \cdot \nabla T + \nabla \cdot \mathbf{q} = 0 \quad (1)$$

$$\mathbf{u} = u_r \hat{\mathbf{r}} + u_z \hat{\mathbf{z}} \quad (2)$$

$$\nabla T = \frac{\partial T}{\partial r} \hat{\mathbf{r}} + \frac{\partial T}{\partial z} \hat{\mathbf{z}} \quad (3)$$

$$\nabla \cdot \mathbf{q} = \frac{1}{r} \frac{\partial r q_r}{\partial r} + \frac{\partial q_z}{\partial z} \quad (4)$$

where:

\mathbf{q} : Conductive heat flux vector in W/m^2

\mathbf{u} : Fluid velocity vector in m/s

$\hat{\mathbf{r}}$ and $\hat{\mathbf{z}}$: Unit radial and axial vectors

u_r and u_z : Velocity vector components

q_r and q_z : Conductive heat flux vector components

r and z : Radial and axial coordinates

T : Temperature of the material in K

ρ : Density of the material in kg/m^3

C_p : Specific heat capacity at constant pressure of the material in J/Kg.K

t : Time in s

Heat transfer between the formation and the grout or casing is assumed to be by conduction and there is no fluid flow in the pores of the formation. Similarly, heat is dissipated and lost from the descending fluid in the annulus and the ascending fluid in the inner pipe by conduction through the inner pipe (and the inner pipe gap). Therefore, the convection/advection term in the general equation (1) is dropped when modeling the heat transfer in the solid domains of the model. Moreover, thermal expansion of the solid domains is neglected. Hence, the simplified general equation for heat transfer in the solid domains is given by

$$\rho C_p \frac{\partial T}{\partial t} + \nabla \cdot \mathbf{q} = 0 \quad (5)$$

As for the heat transfer in the working fluid, the mode of heat transfer is by conduction and convection due to fluid flow. Heat source, pressure work, and viscous dissipation are assumed to be negligible, hence the general equation that models the

heat transfer in the working fluid domain is given by equation (1). For steady state studies, the first term to the left-hand side of equations (1) & (5) is dropped. Fluid flow equations are required to model the fluid velocity vector (\mathbf{u}). Therefore, the heat transfer equations are fully coupled with the fluid flow equations (mainly equation (12)) in section 3.2.2.

Whenever a PCM is added to the gap inside the inner pipe, it undergoes phase changes as it stores and releases thermal energy in the form of latent heat. Air and PCM inside the inner pipe gap are assumed to be steady state ($u=0$ m/s), hence, the equation that governs heat transfer in this domain is equation (5). The PCM has a specific heat capacity at constant pressure and thermal conductivity given by

$$C_p = \theta_1 C_{p,1} + \theta_2 C_{p,2} + \frac{1}{2} L_{1 \rightarrow 2} \frac{\partial(\theta_2 - \theta_1)}{\partial T} \quad (6)$$

$$k = \theta_1 k_1 + \theta_2 k_2 \quad (7)$$

where:

$C_{p,1}$: Specific heat capacity at constant pressure of the material in phase 1 in J/Kg.K

$C_{p,2}$: Specific heat capacity at constant pressure of the material in phase 2 in J/Kg.K

$L_{1 \rightarrow 2}$: Latent heat capacity of the material in J/Kg

θ_1 : Fraction of phase 1

θ_2 : Fraction of phase 2

$T_{pc,1 \rightarrow 2}$: Phase change temperature in K

$\Delta T_{1 \rightarrow 2}$: Phase change temperature range in K

Figure 9 illustrates the phase change between phase 1 and phase 2.

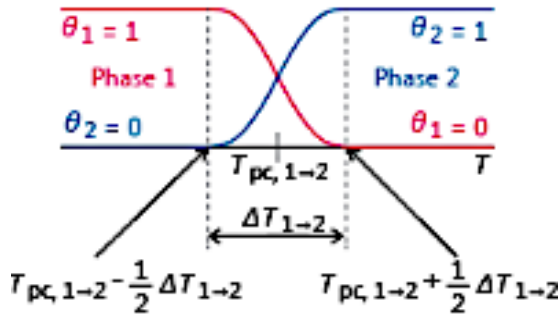


Figure 9 Phase change profile of the PCM (taken from COMSOL)

3.2.2. Fluid Flow Model Equations

Reynold's number is used to determine if the fluid flow is laminar or turbulent, and is given by

$$Re = \frac{\rho u D}{\mu} \quad (8)$$

The characteristic diameter of the coaxial BHE sections are as follows:

$$D = \begin{cases} D_i & \text{For the inner pipe} \\ D_c - D_o & \text{For the annulus} \end{cases}$$

where:

Re : Dimensionless Reynolds number

ρ : Density of the fluid in kg/m^3

u : Fluid inlet velocity in m/s

μ : Dynamic viscosity in $\text{Pa}\cdot\text{s}$ or in $\text{Kg/m}\cdot\text{s}$

D : Characteristic diameter in m

The inlet mass flowrate used in the model is 0.5 Kg/s equivalent to 0.041 m/s , and the characteristic diameter at the inlet is 5 cm . Water density and dynamic viscosity at 288.15 K are 999.1 Kg/m^3 and $0.0011375 \text{ Pa}\cdot\text{s}$, respectively. By substituting the values in equation (8) the resulting Reynolds number is 1800 which implies that the fluid flow

is in the laminar range. The Navier-Stokes equation is used to model the flow in the coaxial BHE, the equation includes the inertial forces on the left-hand side. On the right-hand side of the equation the pressure forces, viscous forces, external forces, and gravity forces are represented in the first, second, third, and last term respectively as follows:

$$\rho \left(\frac{\partial \mathbf{u}}{\partial t} + \mathbf{u} \cdot \nabla \mathbf{u} \right) = \nabla \cdot [-p\mathbf{I} + \mu(\nabla \mathbf{u} + (\nabla \mathbf{u})^T)] + \mathbf{F} + \rho \mathbf{g} \quad (9)$$

$$\nabla \mathbf{u} = \frac{\partial u}{\partial r} \hat{\mathbf{r}} + \frac{\partial u}{\partial z} \hat{\mathbf{z}} \quad (10)$$

For incompressible fluid flow, the continuity equation is incorporated:

$$\rho \nabla \cdot (\mathbf{u}) = 0 \quad (11)$$

where:

\mathbf{u} : Fluid velocity vector in m/s

$$\mathbf{I}: \text{Identity matrix} = \begin{pmatrix} 1 & 0 & 0 \\ 0 & 1 & 0 \\ 0 & 0 & 1 \end{pmatrix}$$

\mathbf{F} : Body external force vector in N/m³

\mathbf{g} : Gravitational acceleration vector in m/s²

$\hat{\mathbf{r}}$ and $\hat{\mathbf{z}}$: Unit radial and axial vectors

t : Time in s

p : Contact pressure in Pa

μ : Dynamic viscosity in Pa.s or in Kg/m.s

ρ : Density of the fluid in kg/m³

r and z : Radial and axial coordinates

The body external forces are assumed to be negligible, consequently; the corresponding term is dropped from the Navier-Stokes equation:

$$\rho \left(\frac{\partial \mathbf{u}}{\partial t} + \mathbf{u} \cdot \nabla \mathbf{u} \right) = \nabla \cdot [-p\mathbf{I} + \mu(\nabla \mathbf{u} + (\nabla \mathbf{u})^T)] + \rho \mathbf{g} \quad (12)$$

Initial pressure at any point in the system is given by the following equation:

$$p_{\text{init}} = p + p_{\text{hydro}} \quad (13)$$

The hydrostatic pressure of the working fluid column is given by the following equation:

$$p_{\text{hydro}} = \rho_{\text{ref}} \mathbf{g} \cdot (\mathbf{z}_{\text{ref}} - \mathbf{z}) = -\rho_{\text{ref}} \mathbf{g} \cdot \mathbf{z} \quad (14)$$

The reference point and the fluid inlet are selected at $z_{\text{ref}}=0$

where:

\mathbf{g} : Gravitational acceleration vector in m/s^2

p_{init} : Initial pressure at any point in the system in Pa

p : Pressure at the reference in Pa

p_{hydro} : Hydrostatic pressure in Pa

\mathbf{z} : Vertical height in m

\mathbf{z}_{ref} : Elevation of the reference in m

ρ_{ref} : Fluid density at the reference in kg/m^3

3.2.2 Numerical Approach

COMSOL Multiphysics software uses the finite element approach to solve the heat transfer and fluid flow equations [41]. In study 1, equation (12) is solved for steady state where the time dependent term is neglected. The steady state values of the velocity and pressure fields from study 1 are taken as initial values in the transient study 2 where equations (1) and (5) are being solved for. This facilitates the convergence, since the flow is considered laminar (despite the arguments discussed in sections 3.3 and 3.7), moreover, the velocity field reaches a steady state very early relative to the simulated

duration over 60 years. COMSOL Multiphysics uses the stabilization method of Anderson acceleration by default and a constant (Newton) nonlinear method with a damping factor of 0.9 [41], [42]. The used default verification helps avoid fluctuations in the numerical solution in most cases. To further improve the solution in other cases, the mesh size and/or tolerance can be decreases, however, this results in higher computational time. Since the interest is in the energy budget, small numerical fluctuations will not affect the overall physics. The relative tolerance is set as physics controlled by default and the absolute tolerance is set by scaled global method where a tolerance factor of 0.1 is used. Using adaptive time stepping, the time stepping follows the backward differentiation formula (BDF). The used solver for transient simulations is PARDISO with automatic reordering algorithm.

3.3. Model Domain Materials and Properties

The materials used in each domain of the model are similar to the ones studied by Caulk & Tomac, 2017 [6] which includes the inner pipe insulation properties. The density and specific heat capacity of the inner pipe are taken similar to the ones of polyethylene which is the most used. The model domain materials and their respective properties are listed in Table 6. Furthermore, grout is added to the model to study the influence of its properties on the well performance. Two types of grouts are tested which are the conventional grout (commercial bentonite) and thermally enhanced grout (bentonite with thermally enhancing additive). The properties of the grout materials are taken from the study by Delaleux et al. [43].

Table 6 Materials used in each domain and their corresponding properties (COMSOL Material Library, [6], & [43])

Domain	Material	Thermal Conductivity k (W/m.K)	Density ρ (Kg/m ³)	Heat Capacity C_p (J/Kg.K)
Formation	Sedimentary rock	2.9	2650	780
Casing	Steel	50	7950	420
Working Fluid	Water	$[-0.8691 + 8.95 \times 10^{-3} \times T - 1.584 \times 10^{-5} \times T^2 + 7.97 \times 10^{-9} \times T^3]$	For $0^\circ\text{C} < T < 20^\circ\text{C}$ $[6.31 \times 10^{-5} \times T^3 - 6 \times 10^{-2} \times T^2 + 18.923 \times T - 950.7]$ For $20^\circ\text{C} < T < 100^\circ\text{C}$ $[1 \times 10^{-5} \times T^3 - 1.34 \times 10^{-2} \times T^2 + 4.9693 \times T + 432.26]$	$[3.6254 \times 10^{-7} \times T^4 - 5.382 \times 10^{-4} \times T^3 + 0.31 \times T^2 - 80.41 \times T + 12010.15]$
Inner Pipe	Polyethylene	0.1	2300	1500
Grout 1	Commercial bentonite (Scenario 2)	1.5	2500	1500
Grout 2	Bentonite with 5 wt.% compressed expanded natural graphite (Scenario 2)	5	2500	1500
Gap	Air (Scenario 3)	$[-7.44 \times 10^{-15} \times T^4 + 4.12 \times 10^{-11} \times T^3 - 7.9 \times 10^{-8} \times T^2 + 1.15 \times 10^{-4} \times T - 2.3 \times 10^{-3}]$	$\frac{1}{R} \left[\frac{\partial(0.02897 \cdot T \cdot P_A)}{\partial P_A} + \frac{\partial(0.02897 \cdot T \cdot P_A)}{\partial T} \right]$	$[1.286 \times 10^{-10} \times T^4 - 6.024 \times 10^{-7} \times T^3 + 9.453 \times 10^{-4} \times T^2 - 0.3726 \times T + 1047.64]$

The dynamic viscosity of the working fluid varies with temperature according to the following equations (COMSOL Material Library):

$$\mu \begin{cases} \text{for } 0^\circ\text{C} < T < 140^\circ\text{C} \\ 3.85 - 0.0592 \times T + 3.79 \times 10^{-4} \times T^2 - 1.296 \times 10^{-6} \times T^3 + 2 \times 10^{-9} \times T^4 \\ \quad - 2.533 \times 10^{-12} \times T^5 + 1.073 \times 10^{-15} \times T^6 \\ \text{for } 140^\circ\text{C} < T < 280.6^\circ\text{C} \\ 0.0112 - 5.88 \times 10^{-5} \times T + 1.08 \times 10^{-7} \times T^2 - 6.688 \times 10^{-11} \times T^3 \end{cases}$$

In this study, turbulence is ignored as some studies in the literature assumed laminar flow and have proven to generate results comparable to field application results [6].

3.4. Initial and Boundary Conditions

The model initial and boundary conditions are illustrated in Figure 10. Dirichlet boundary conditions are imposed on the model boundaries. The top formation boundary has an ambient temperature of 15°C, the well inlet fluid temperature is 15°C, and the formation crustal geothermal gradient temperature is assumed 7°C/100 m. The formation temperature is represented by the following equation:

$$T_f = an1(z) = T_{surf} + G.G * (-z) = 15 - 0.07z \quad (15)$$

where:

T_f : Formation temperature in °C

T_{surf} : Surface ambient temperature in °C

$G.G$: Geothermal gradient in °C/m

z : Depth in m (negative since the reference is taken at $z=0$ m)

A Neumann heat flux boundary condition of 0.075 W/m² is set at the bottom formation boundary to model the crustal heat flow. According to the sensitivity analysis performed by Caulk & Tomac, 2017 [6], the lowest inlet mass flowrate (1 kg/s) yielded the highest outlet temperature of 32.96°C for a 7°C/100 m geothermal gradient. In the current study, an inlet mass flowrate of 0.5 kg/s is used which yields a laminar fluid flow and a high outlet temperature. A constant pressure boundary condition of 0 Pa is set at the outlet of the coaxial geothermal well model. Furthermore, a no slip boundary condition is set in the fluid flow domain where the fluid velocity is 0 m/s at the casing and inner pipe walls.

The temperature initial conditions of the model are defined as follows: the temperature initial condition of the formation is set equal to the crustal temperature

gradient represented in equation (15). The well domain including the working fluid has an initial temperature equal to the fluid inlet temperature of 15°C. For the flow initial conditions, the fluid domain has an initial velocity of 0 m/s in both the r and z directions. The initial pressure of the fluid system is equal to the hydrostatic pressure as indicated in equation (13) and equation (14). The fluid flow is set in a reverse circulation mode (i.e., fluid is injected from annulus and produced through the inner pipe).

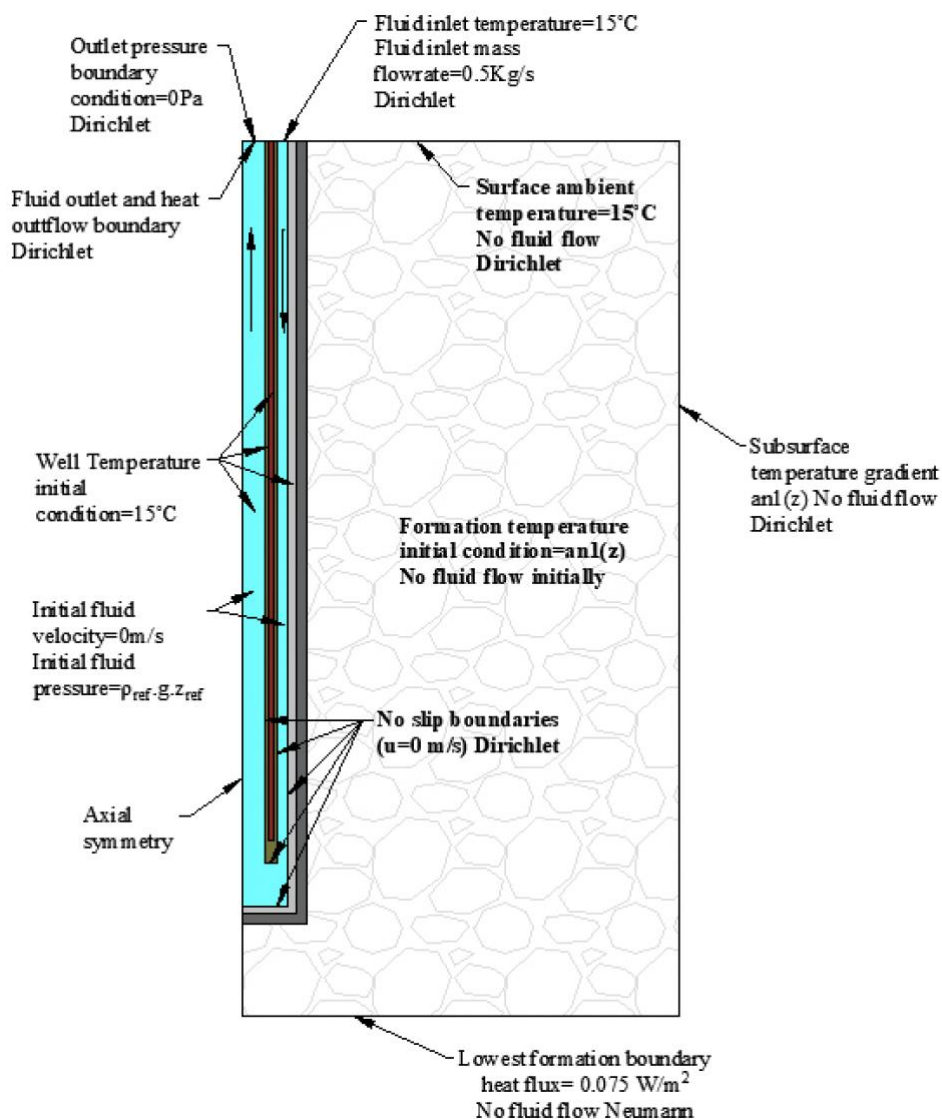


Figure 10 Model initial and boundary conditions

3.5. Modeling Scenarios

3.5.1. Scenario 1: Base Model

The model with thin inner pipe studied by Caulk & Tomac, 2017 [6] was simulated for verification purpose. The thickness of the inner pipe is increased to 1 cm and 2 cm to assess the influence of inner pipe thickness on the well performance. Afterwards, the model with 2 cm thick inner pipe is used as a base model for a comparative study with the models with an air gap, PCM gap, and grout.

3.5.2. Scenario 2: Model with Grout

In scenario 2, a 3 cm thick grout domain is added to the base model. Two types of grouts are modeled: (1) the commercial conventional bentonite and (2) a thermally enhanced grout composed of bentonite with 5 wt.% compressed expanded natural graphite.

3.5.3. Scenario 3: Model with Inner Pipe Air Gap

An air gap with different heights is added to the inner pipe to study its influence on the performance of the well. Three air-filled gap height (L_{air}) are considered: $L_{air} = 200$ m, 400 m, and 999.75 m (i.e., the air gap extends to the bottom of the inner pipe). For each case, the steady state and transient temperatures are calculated and compared with the base model.

3.5.4. Scenario 4: Model with Inner Pipe PCM Gap

A 50 m height of PCM is included in the inner pipe gap to illustrate the efficiency of PCM on the performance of coaxial geothermal wells.

The PCM melting temperature must fall in the temperature range of the inner pipe section to ensure both the melting and solidification of the PCM. For PCM selection in the inner pipe gap, it is preferable that the selected PCM has low thermal conductivity to avoid heat loss from the fluid in the inner pipe to that in the annulus. Additionally, the selected PCM should have high melting enthalpy per volume unit, high specific heat and density. Moreover, it is favourable that the volume change of the material due to phase change is negligible [46].

3.6. Performance and Economic Evaluation Methodology

The well performance is evaluated through the estimation of the output power which is the well power capacity. According to He et al. [47], the output power of the geothermal well model can be estimated through the following equation:

$$W_{out} = c_{out}\dot{m}_{out}T_{out} - c_{in}\dot{m}_{in}T_{in} \quad (16)$$

where:

W_{out} : Output power in J/s

c_{out} : Heat capacity of the working fluid at the outlet in J/Kg.K

T_{out} : Outlet temperature in K

\dot{m}_{out} : Outlet mass flowrate in Kg/s

c_{in} : Heat capacity of the working fluid at the inlet in J/Kg.K

T_{in} : Inlet temperature in K

\dot{m}_{in} : Inlet mass flowrate in Kg/s

The flow is continuous, hence the fluid mass injected in the system is equal to that produced and

$$\dot{m}_{in} = \dot{m}_{out} = 0.5 \frac{Kg}{s} \quad (17)$$

The heat capacity of water varies with temperature as follows:

$$c_p = 12010.15 - 80.41 * T + 0.3099 * T^2 - 5.382 \times 10^{-4} * T^3 + 3.6254 \times 10^{-7} * T^4 \quad (18)$$

The inlet temperature T_{in} of the working fluid is 288.15 K, hence, $c_{in} = 4193.95$ J/Kg.K

By substituting the previous data in equation (16), the output power of the system can be calculated from the outlet temperature as follows:

$$W_{out} = -604243.346 + 6005.075 * T_{out} - 40.205 * T_{out}^2 + 0.15495 * T_{out}^3 - 2.691 \times 10^{-4} * T_{out}^4 + 1.8127 \times 10^{-7} * T_{out}^5 \quad (19)$$

The variation of the well output power is plotted with respect to time for all of the simulated models. Afterwards, the annual thermal energy output of the well models is plotted over the models' lifetime. Annual thermal energy output is the integral of the output power per year interval. Then, the overall thermal energy output of the well models is calculated by summing the annual thermal energy output over the well lifetime. The overall thermal energy output value is used to compare the different models.

The economic analysis is measured using the levelized cost of energy (LCOE) for each well. The LCOE is the lifetime cost of the well (including drilling, completion, operation, and maintenance) divided by the amount of energy produced. This gives an indication of how much it costs to produce 1kWh of energy from each well model. The model with the lowest LCOE value is considered the most economically feasible.

3.7. Assumptions and Limitations

For the purpose of simplifying the model and reducing the computational time and power, the following assumptions are made:

- The solid domains in the model (i.e., formation, grout, casing, and the inner pipe) are assumed to be uniform.
- Heat transfer between the formation and the grout is by conduction only, formation water is assumed to be absent or steady state if present.
- Due to the fact that the steel casing has a very high thermal conductivity, the thickness of the casing is neglected (assumed as a layer with corresponding casing properties) to reduce number of mesh elements and eventually computational time.
- Fluid inlet velocity is assumed to be in the laminar range to model the fluid flow using the laminar flow interface, and turbulence is neglected in the well.
- The mechanical stresses involved around the inner pipe and the casing are neglected. Geothermal wells with no grout do not exist, model with no grout is used for comparison purpose in this study.
- The economic analysis performed uses a simple approach to obtain rough estimations of costs for comparison purposes. A more thorough and detailed analysis should be performed for each model.
- The formation temperature increases linearly with depth.

CHAPTER 4

RESULTS AND DISCUSSION

4.1. Model Benchmark

The model is benchmarked against the steady state model developed by Caulk & Tomac, 2017 [6], by doing a comparison to 24 steady state models with different geothermal gradients, mass flowrates, and number of mesh elements. The results are described in Table 7 and show that the relative difference is less than 5%.

To optimize the computational time and ensure accurate results, a sensitivity analysis on mesh size is performed and reported in the APPENDIX. Furthermore, it was found that for a domain width of 200 m the results of the steady state model converge similarly to what was found by Caulk & Tomac, 2017 [6].

Table 7. Model benchmark results against Caulk & Tomac, 2017 [6]

Well Depth (m)	Geothermal Gradient (°C/m)	Mass Flowrate (kg/s)	Outlet Temperature (°C) Reported by Caulk & Tomac, 2017	Current Study Outlet Temperature in °C and Relative Difference in %									
				Number of Mesh Elements	1,724,285		1,110,896		849,347		674,555		
1000	4.5	1	26.36	Current Study Simulation Results	26.39	0.11%	26.38	0.08%	26.38	0.08%	26.42	0.22%	
		4.4	18.51		18.48	0.17%	18.02	2.67%	18.5	0.06%	18.51	0.03%	
		10	16.31		16.58	1.66%	16.42	0.7%	16.44	0.78%	16.49	1.1%	
	7	1	32.96		32.57	1.17%	32.78	0.55%	32.6	1.09%	32.65	0.93%	
		4.4	19.64		20.45	4.11%	20.45	4.1%	20.17	2.68%	20.63	5.04%	
		10	16.97		17.46	2.88%	17.39	2.49%	17.32	2.08%	17.47	2.92%	

4.2. Results

4.2.1. Scenario 1: Inner Pipe Thickness Analysis

Figure 11 shows the outlet temperature over 60 years of the models with different inner pipe thicknesses. The temperature at the outlet increases rapidly from its initial value of 15°C for all models until reaching a maximum temperature, beyond which drops gradually. It can be observed that increasing the inner pipe thickness significantly improves the geothermal well performance. Increasing the inner pipe thickness from 1 cm to 2 cm improved the outlet temperature by 6-8°C. Thickening the inner pipe significantly reduced the heat lost from the inner pipe to the annulus by conduction and eventually increased the harvested thermal energy.

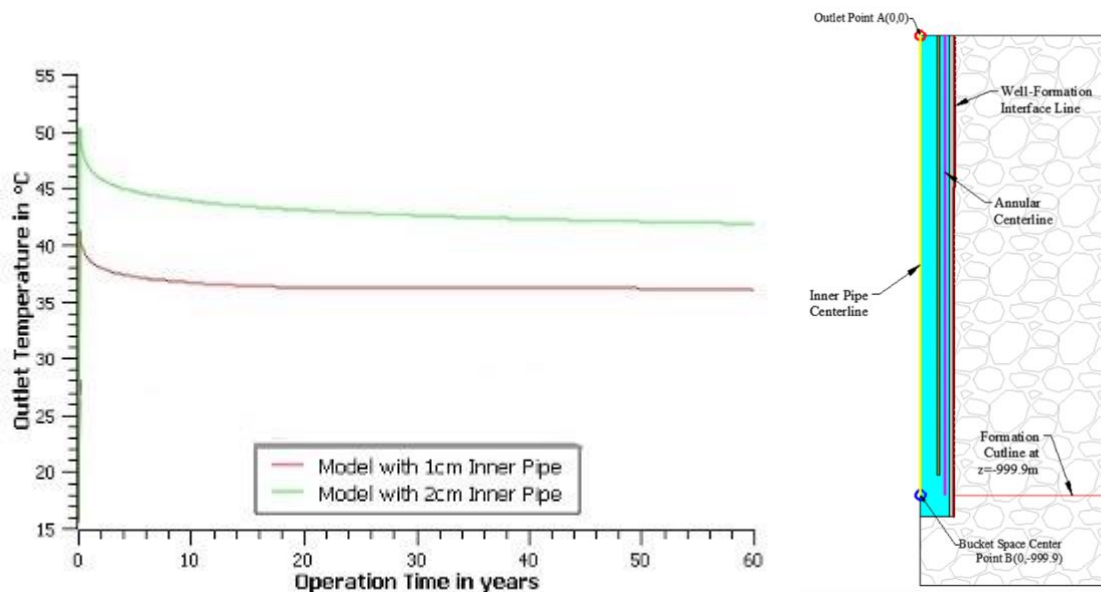


Figure 11 Variation of outlet temperature with time (Point A) for models in scenario 1

Similarly, Figure 12 shows that the temperature in the bucket space (point B in Figure 7) significantly dropped after increasing the inner pipe thickness. This can be attributed to the lower quantity of heat being transferred from the inner pipe to the

annulus by conduction due to thicker inner pipe, and the main source of heat exchange is from the formation rather than from both the formation and the inner pipe.

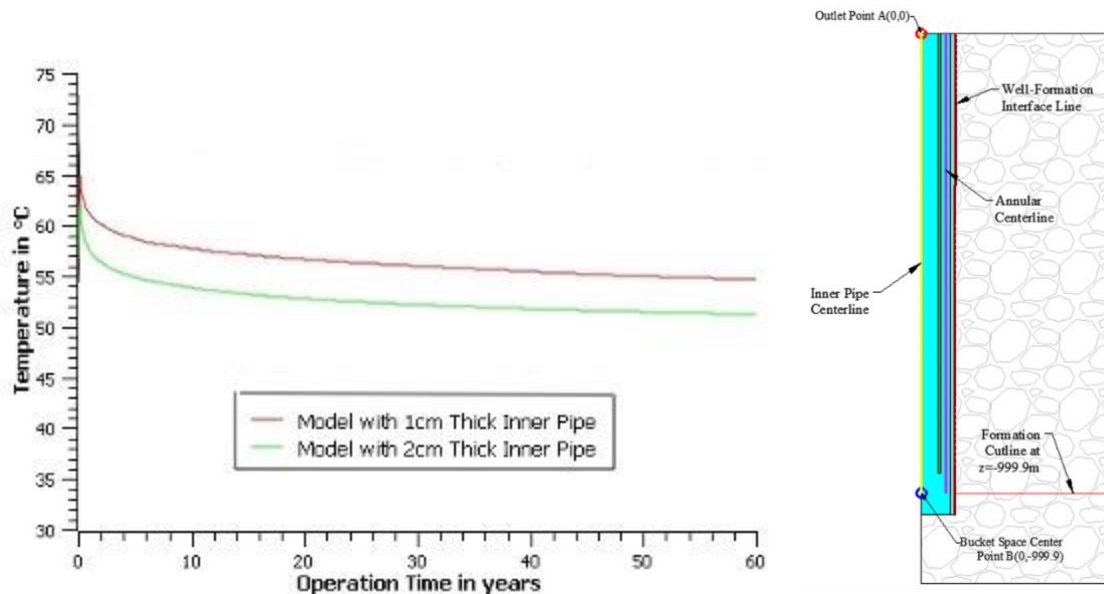


Figure 12 Variation of temperature with time in the bucket space (Point B) for models in scenario 1

Figure 13 shows the temperature profile along the centerline of the inner pipe which drops with time for all of the simulated models. It can be observed that the slope of temperature drop in the model with 1 cm thick inner pipe is higher than that of the model with 2 cm thick inner pipe. This confirms as expected that increasing the inner pipe thickness reduces heat losses from the inner pipe. Moreover, the results show a crossover of the temperature curves between the depths of 400 m and 600 m. This indicates that the outlet temperature can be improved by modifying the effective properties of the inner pipe (thickness, thermal conductivity, latent heat of fusion whenever a PCM is used) for depths shallower than 600 m. This was shown in section 4.2.3. Scenario 3: Inner Pipe Air Gap Analysis.

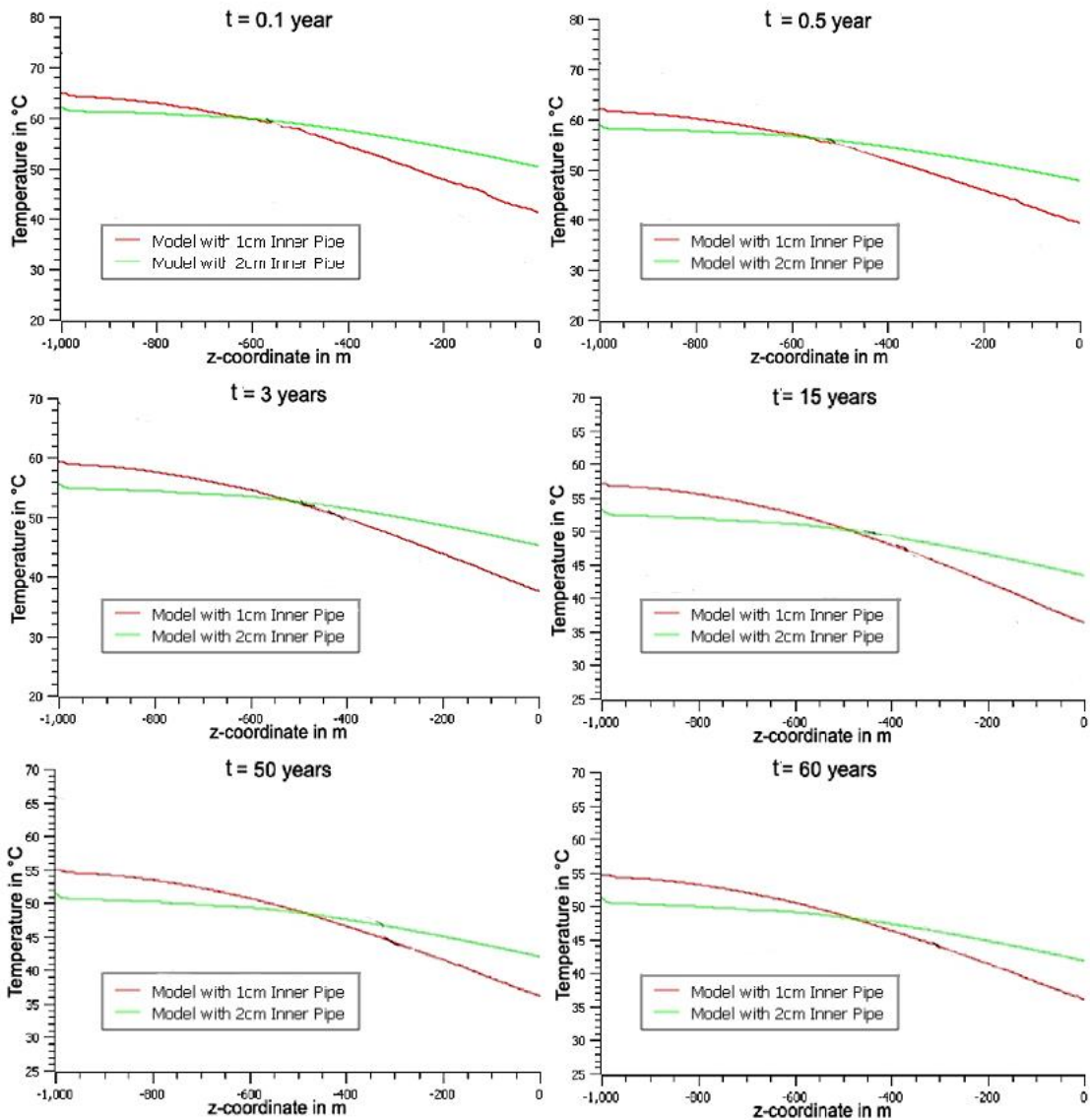


Figure 13 Variation of temperature along the inner pipe centerline at different operation times for models in scenario 1

4.2.2. Scenario 2: Grout Material Analysis

The influence of grout on the well performance is analyzed by adding a 3 cm thick grout domain to the base model of scenario 1 that includes the 2 cm thick inner pipe. We note that grout needs to be included when the well has a casing for zonal isolation. According to the outlet temperature results shown in Figure 14, the temperature increased from an initial value of 15°C to a maximum temperature after which it drops gradually. It can be observed that the addition of a grout domain of

commercial bentonite has reduced the well performance. The outlet temperature of the model drops by around 1°C after the addition of commercial bentonite. This can be attributed to the relatively low thermal conductivity of commercial bentonite, which does not favor heat extraction from the formation. However, the deployment of thermally enhanced bentonite with higher thermal conductivity (see Table 6) slightly improved the performance of the well (by 0.95°C compared to commercial grout). This indicates that the addition of a thermally enhanced grout (with additives) can enhance the well performance better than commercial grout.

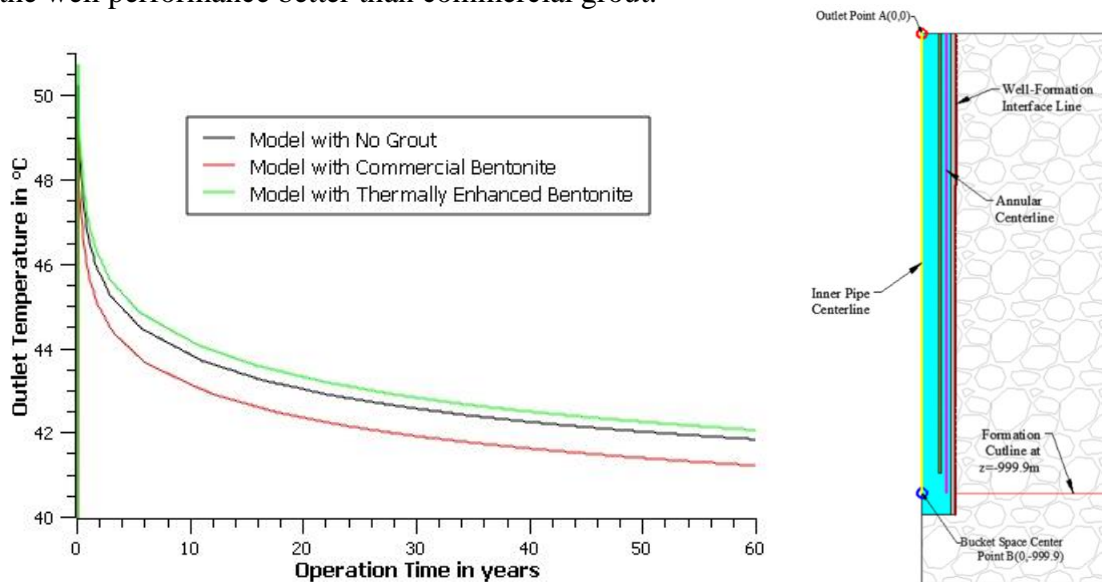


Figure 14 Variation of outlet temperature (Point A) with time for models in scenario 2

Similar observations are made for the bucket space where the temperature drops after the addition of commercial bentonite. Thermally enhanced bentonite improved the bucket space temperature as shown in Figure 15, where heat transfer was enhanced at the bottomhole after the addition of thermally improved grout. The temperature along the annular centerline is plotted in Figure 16 for models with and without grout at 0.5 and 60 years.

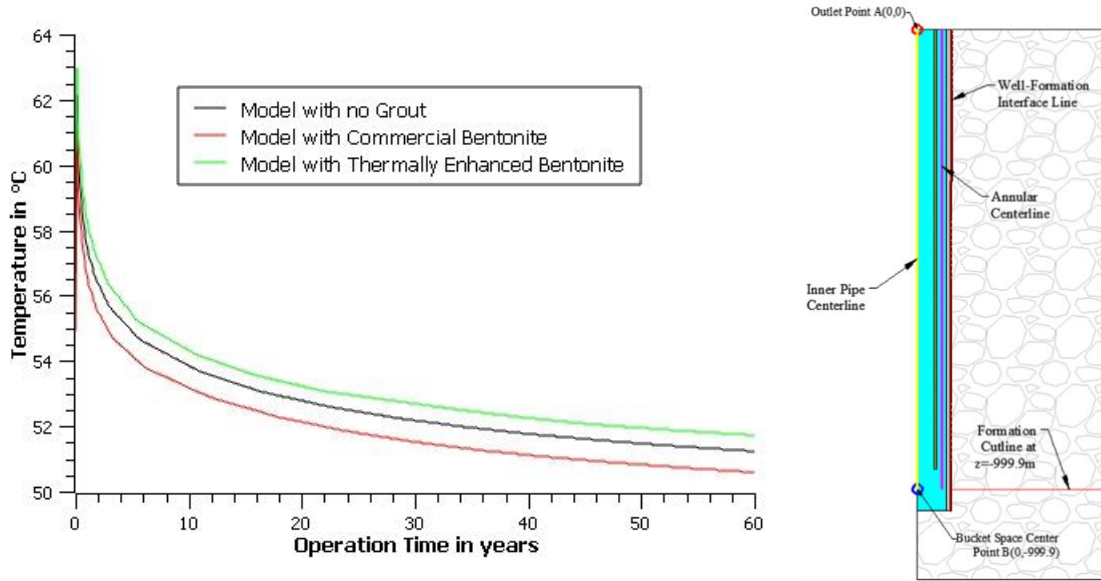


Figure 15 Variation of temperature with time in the bucket space (Point B) for models in scenario 2

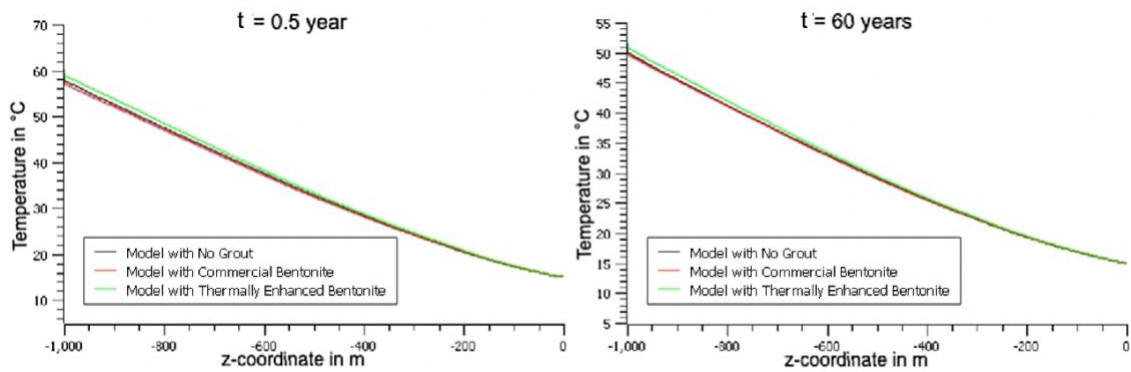


Figure 16 Annular centerline temperature results at $t=0.5$ year (left) and $t=60$ years (right) for models in scenario 2

4.2.3. Scenario 3: Inner Pipe Air Gap Analysis

The coaxial geothermal well model with 2 cm thick inner pipe was simulated without and with 1 cm air gap in the inner pipe. To study the influence of an inner pipe air gap on the geothermal well performance four models were simulated: a model with no air gap and three models with varying air gap depths in the inner pipe including 200 m, 400 m, and 999.75 m.

The variation of outlet temperature with respect to time over 60 years was plotted for all of the simulation models. According to Figure 17, it was found that an air

gap inside the inner pipe improves the outlet temperature of the well in short and long term. The optimal depth for the deployment of an air gap in the inner pipe is 400 m beyond which no significant improvement of the outlet temperature is observed.

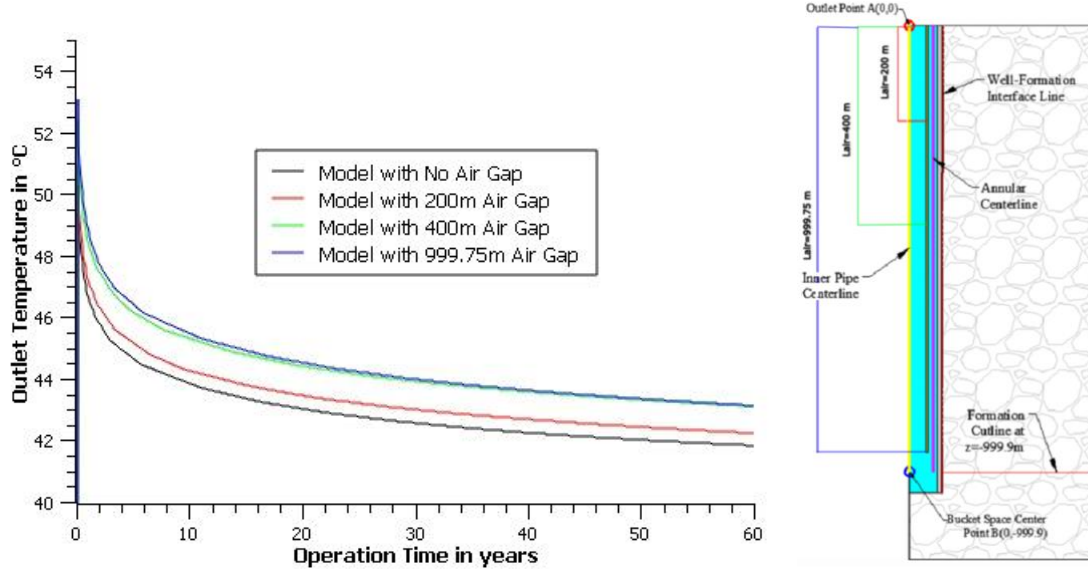


Figure 17 Variation of outlet temperature (Point A) with time for models in scenario 3

The variation of temperature at the center of the bucket space with time for the aforementioned models is shown in Figure 18.

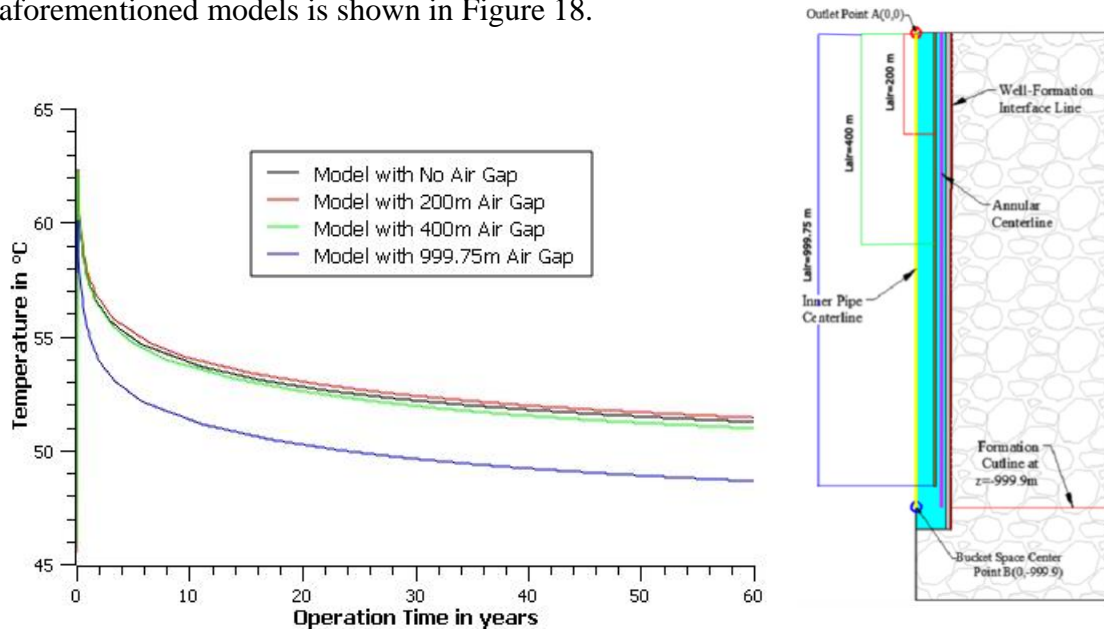


Figure 18 Variation of temperature with time in the bucket space (Point B) for models in scenario 3

It can be observed that increasing the depth of the inner pipe air gap beyond 200 m decreases the temperature at the bucket space. This is due to the lower heat transfer

by conduction occurring from the ascending working fluid in the inner pipe to the descending fluid in the annulus due to air gap.

The temperature along the inner pipe centerline is also analyzed for the aforementioned models at different operation times of 0.1, 0.5, 3, 15, 50, and 60 years. Results are plotted in Figure 19.

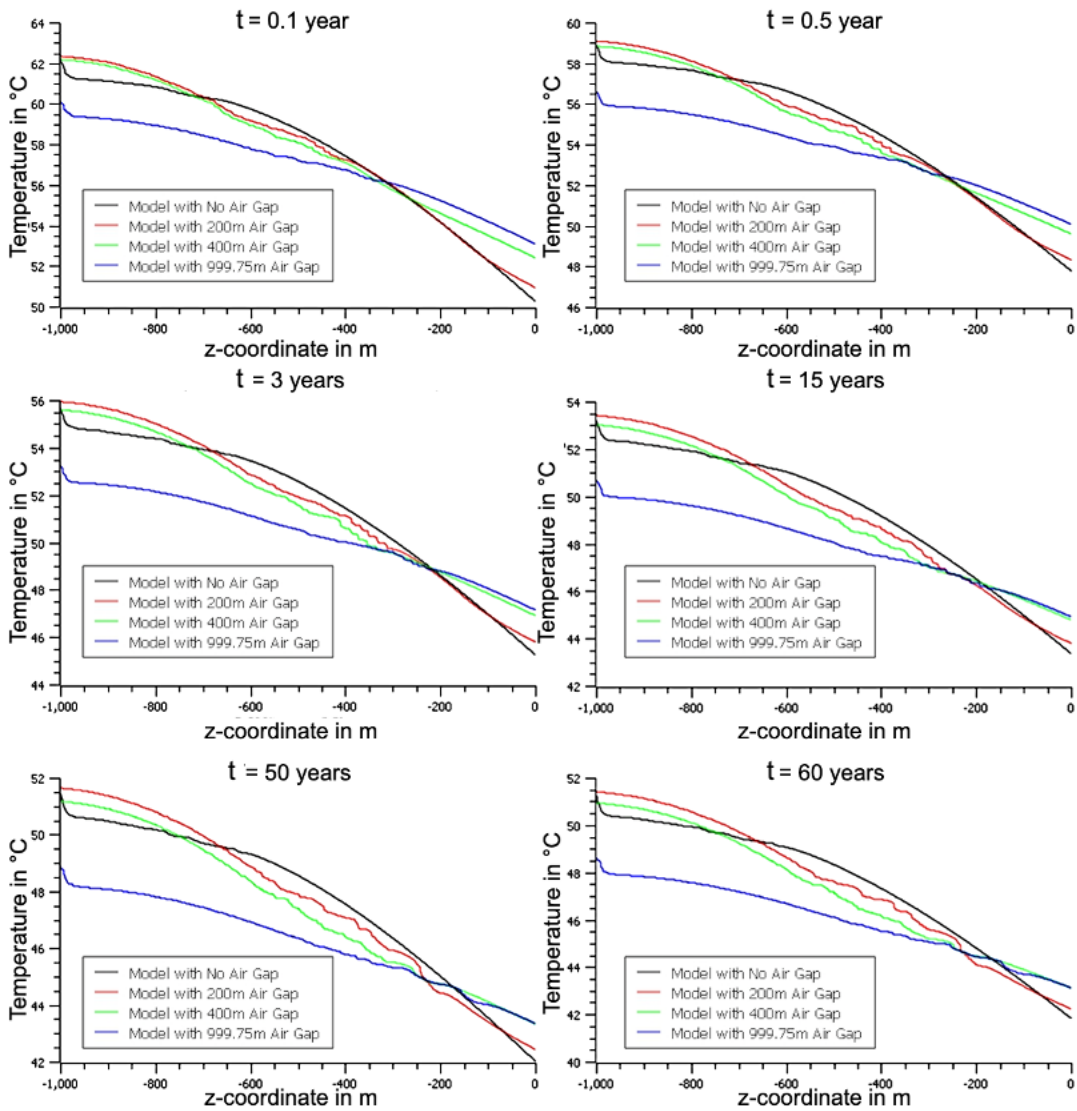


Figure 19 Variation of temperature along the inner pipe centerline at different operation times for models in scenario 3

It can be observed that for all simulated models, the temperature along the inner pipe centerline drops with time. The slope of temperature-depth curve is lowest for the model with 999.75m air gap (air gap extending to the bottom of the inner pipe). This is due to the reduced heat conduction from the inner pipe to the annulus caused by the air gap inside the inner pipe through the entire pipe. As for the models with 200 m and 400 m air gap, the slope of the temperature depth curve starts decreasing at 200 m and 400 m depths respectively. The temperature at depth $z=0$ m for model with 400 m air gap approaches that for model with 999.75 m air gap until they almost overlap at time $t=3$ years (i.e., model with 999.75 m outperforms other models during the first 3 years operation time).

Figure 20 shows the radial variation of temperature with time at depth $z=-999.9$ m for the base model. The radial temperature perturbation reaches a distance of 143m away from the well after 60 years indicating that the selected domain width provides a suitable heat source that mimics actual formation.

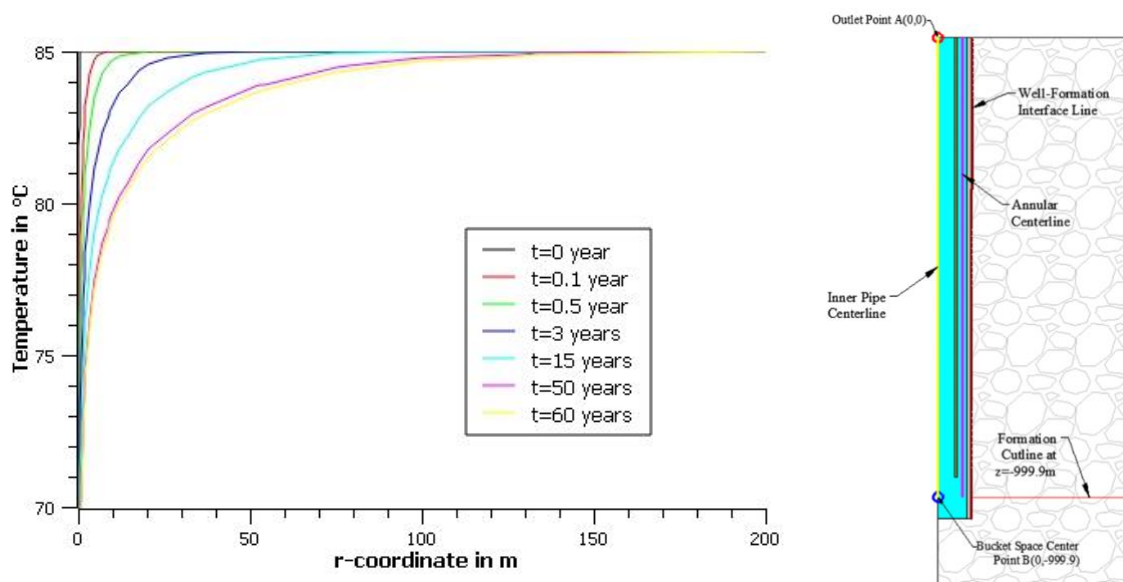


Figure 20 Radial temperature profile of the formation at formation cutline with depth $z=-999.9$ m for base model

Figure 21 shows the radial variation of temperature with time at depth $z=-999.9$ m after 60 years for models with different inner pipe air gap depths. It can be indicated that an air gap in the inner pipe improved the formation temperature around the well allowing a better formation thermal recovery.

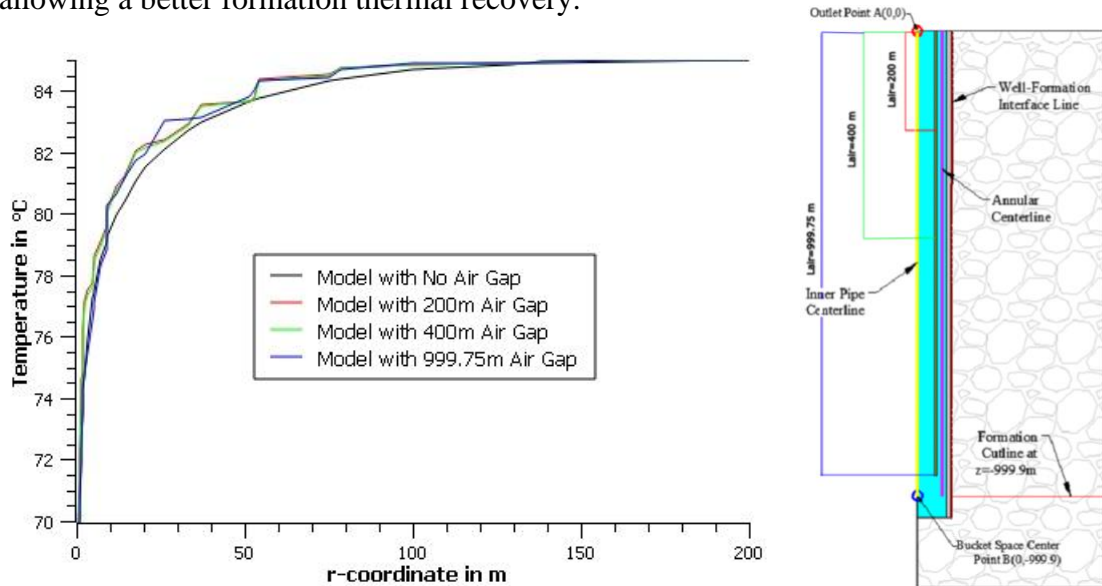


Figure 21 Radial temperature profile of the formation at formation cutline with depth $z=-999.9$ m after 60 years for models in scenario 3

The temperature profiles at the well-formation interface and annular centerline at operation times 0.1, 15, and 60 years are shown in Figure 22 and Figure 23 respectively. It can be observed that the temperature at the well-formation interface and annular centerline drops with time for all simulated models. Temperature dropped further for the model with 999.75m air gap compared to other models. Moreover, increasing the depth of the air gap further dropped the temperature at the interface and annular centerline to lower values. This can be attributed to less heat coming from the inner pipe to the annular space and the interface due to the insulating air gap. The temperature profile at the annular space and interface for models with 200 m and 400 m air gap matches that with 999.75 m air gap at depths 200 m and 400 m respectively.

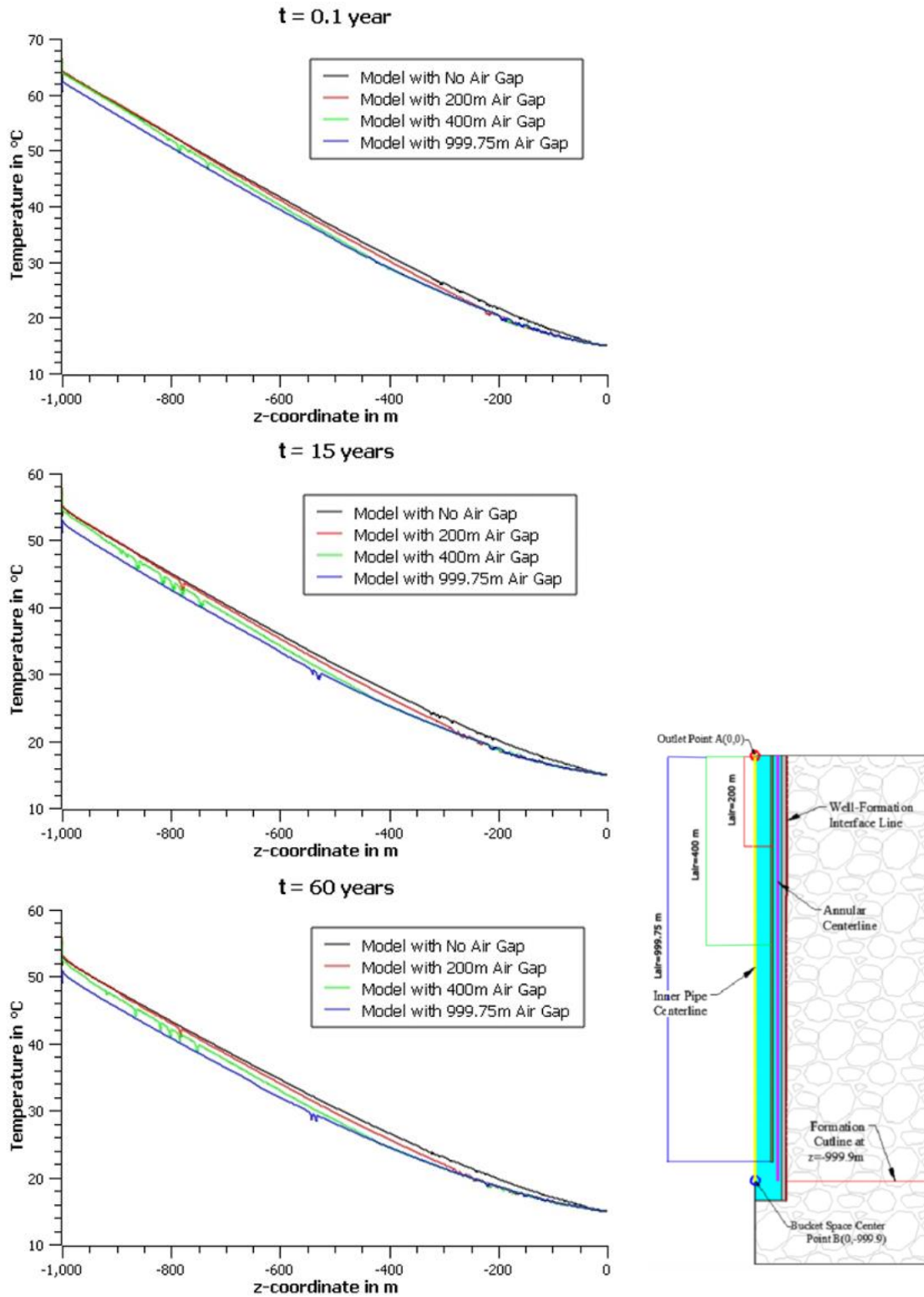


Figure 22 Temperature at the well-formation interface line at operation times 0.1, 15, and 60 years for models in scenario 3

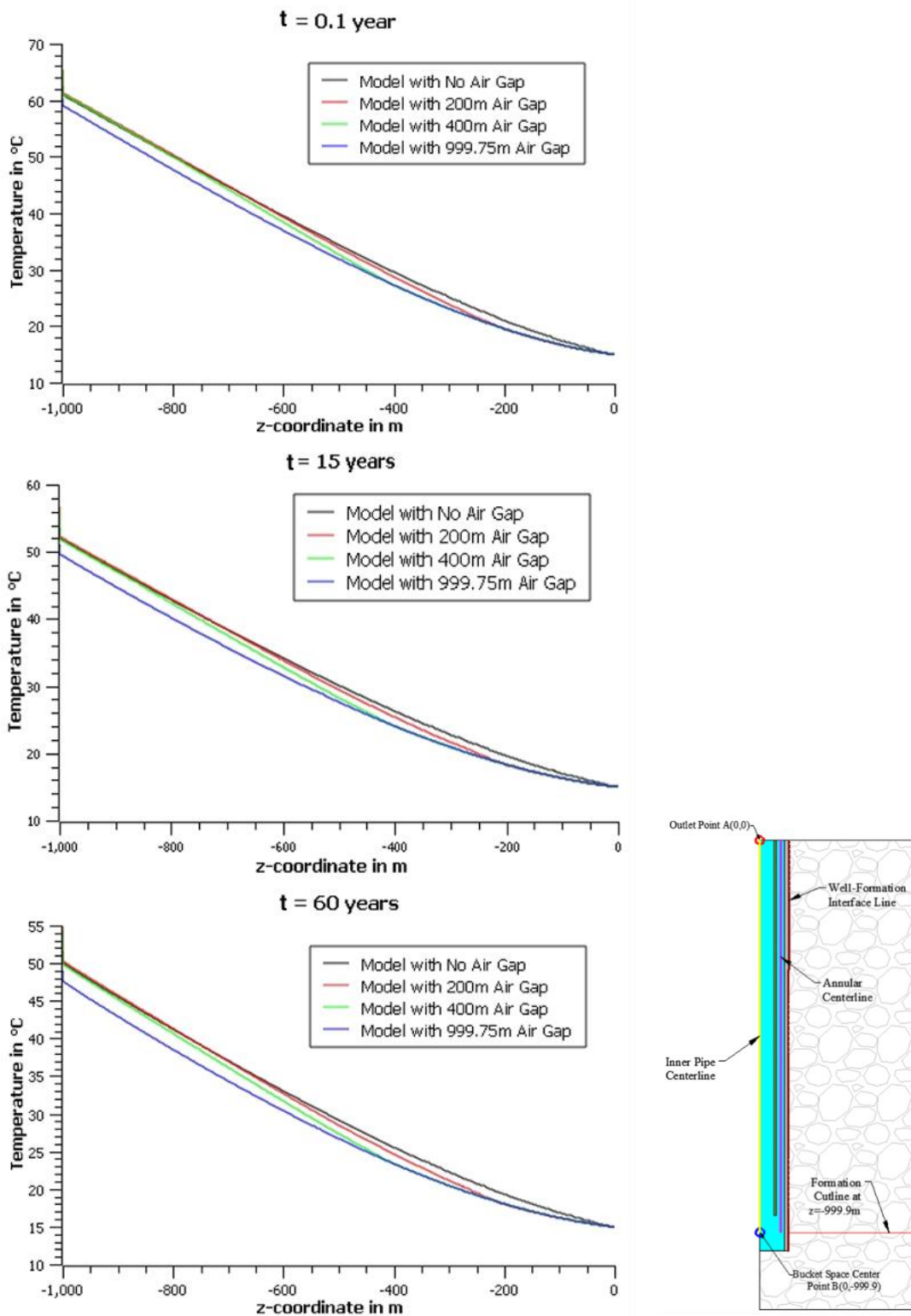


Figure 23 Temperature at the annular centerline at operation times 0.1, 15, and 60 years for models in scenario 3

4.1.4. Scenario 4: Inner Pipe PCM Gap Analysis

To select the best PCM properties and thickness to deploy in the inner pipe we analyze the temperature profile in the first 50 m section of the inner pipe at different operation times (Figure 24) It can be seen that the temperature of the first 50 m section of the inner pipe ranges between 24°C after 60 years and 29°C after 0.1 year of operation time.

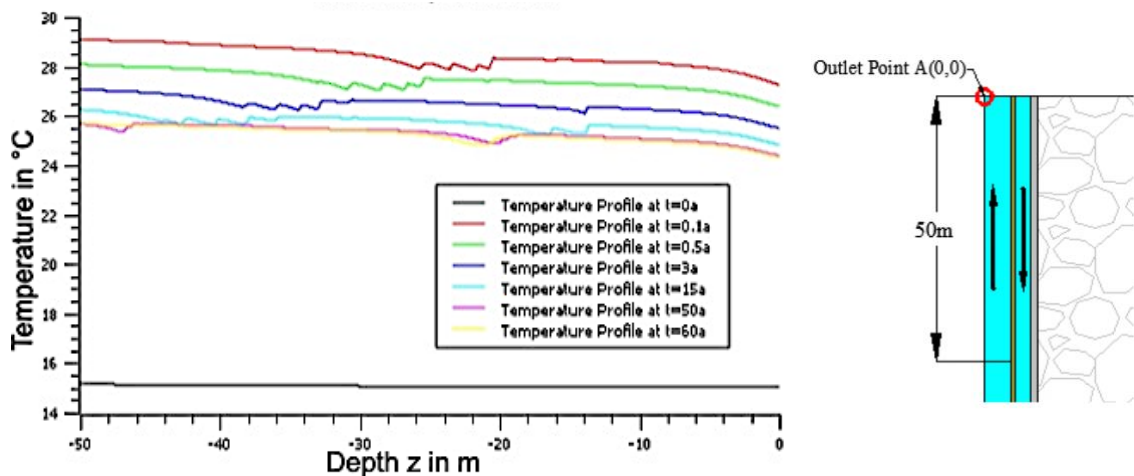


Figure 24 Temperature profile of the first 50 m section of the inner pipe for the base model

Hence, the PCM is selected to have a melting temperature close to the maximum temperature reached in the 50 m section of the pipe. Solid-liquid phase change materials are the most deployed in heat storage applications due to their ability to store latent heat, moreover, their volume change is insignificant compared to liquid-gas PCMs [17]. To deploy a PCM in an inner pipe, it is preferable that the selected PCM has a low thermal conductivity and high latent heat storage. Organic phase change materials are generally characterized by a low thermal conductivity and high thermal and chemical stability [17]. PCM manufacturer PlusICE offer a wide range of PCM of varying melting temperatures and properties as shown in Figure 25.

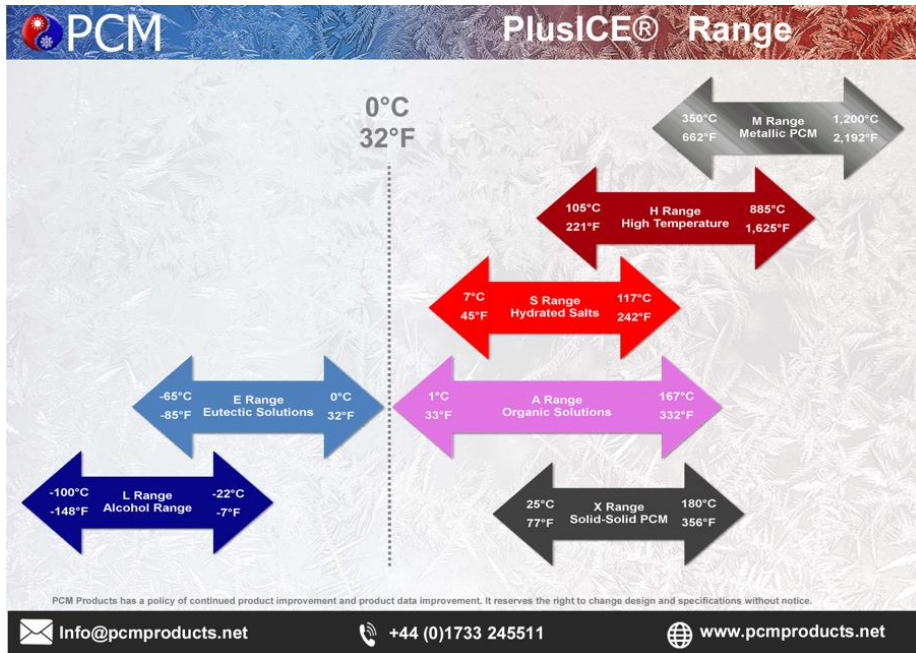


Figure 25 PCM materials offered by PlusICE manufacturer [48]

Table 8 shows the properties of the organic phase change material offered by the manufacturer (PlusICE) and selected for our model. The phase change melting temperature is 28°C with a melting temperature range $\Delta T_{1 \rightarrow 2} = 2^\circ\text{C}$. In this case, the phase change starts at 27°C and stops at 29°C.

Table 8 Properties of the selected PCM chosen based on the inner pipe temperature profile of Figure 24 and the manufacturer (PlusICE)

PCM Type	Phase Change Temperature $T_{pc,1 \rightarrow 2}$ (°C)	Density (Kg/m ³)	Latent Heat Capacity (kJ/kg)	Volumetric Heat Capacity (MJ/m ³)	Specific Heat Capacity (kJ/kg.K)	Thermal Conductivity (W/m.K)	Maximum Operating Temperature (°C)
A28	28	789	265	209	2.22	0.21	200

The outlet temperature for short-term well operation has shown recognizable improvement by 5°C as can be seen from Figure 26. The outlet temperature increases from an initial value of 15°C till it reaches a maximum temperature beyond which it decreases gradually for both models. The reason for outlet temperature fluctuations in the model with PCM is the cyclic melting and cooling of the PCM inside the inner pipe

gap. The temperature drops during the PCM melting phase as it stores latent heat from the ascending working fluid, and it increases during PCM solidification.

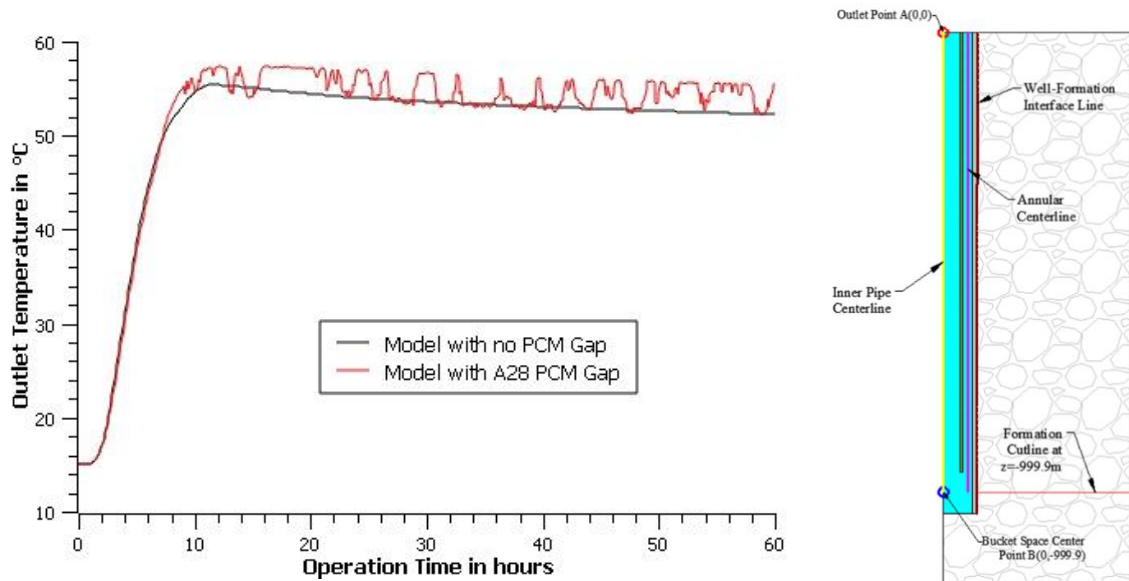


Figure 26 Outlet temperature results (Point A) for models in scenario 4

The phase change profile of the PCM inside the gap is plotted in Figure 27 at different depths over the operation period. It can be observed that significant phase change occurs at depths 10 m and 40 m in the gap. At the surface of the gap, the PCM melted twice before remaining in its liquid phase after 14h of operation time. PCM at 30 m depth in the gap melted once after 10h of operation time and remained in the liquid phase.

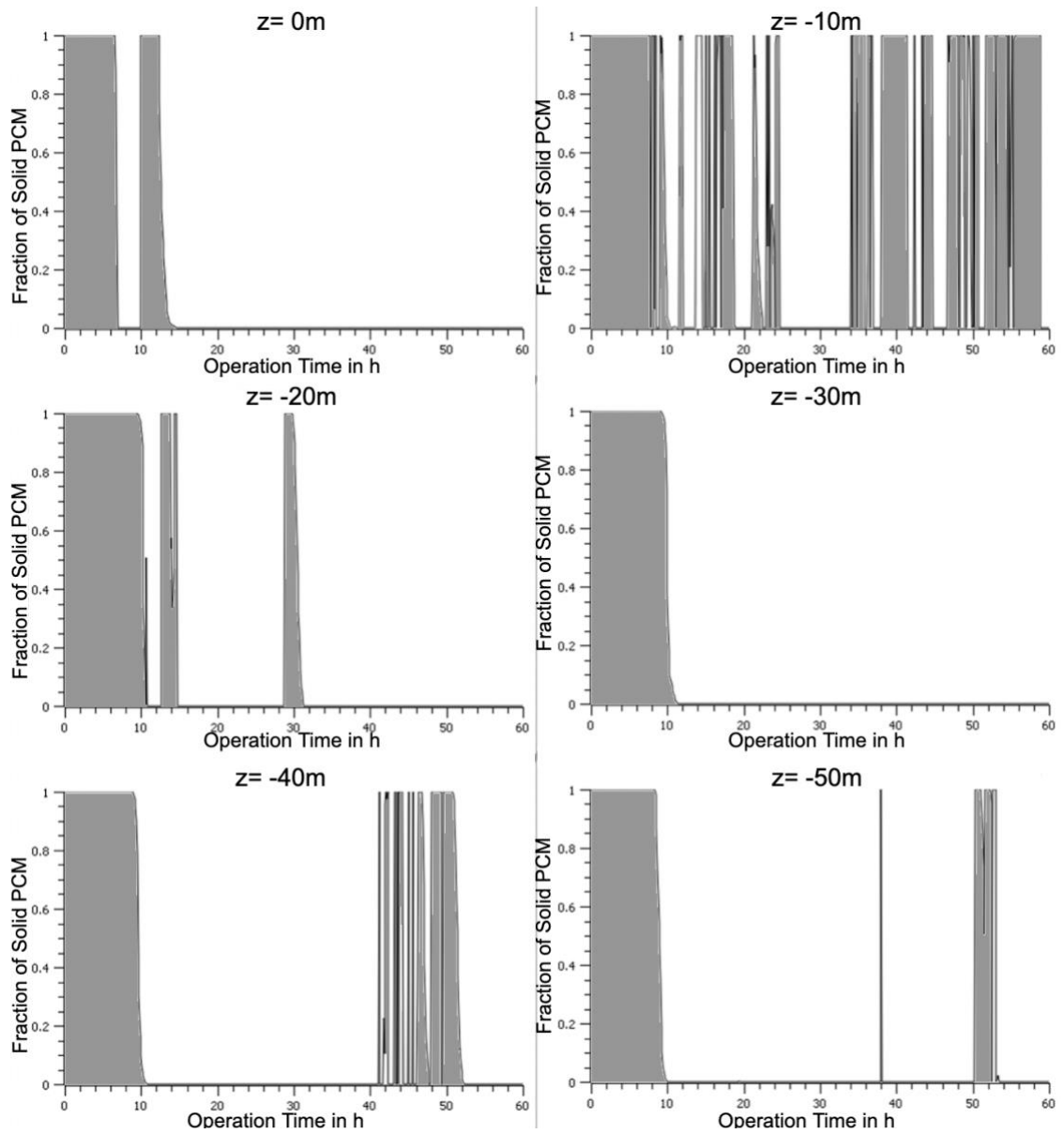


Figure 27 Phase change profile of the PCM at different depths in the gap

4.3. Performance Evaluation of Simulated Models

The variation of thermal energy output with time for models simulated in scenario 1 is plotted in Figure 28.

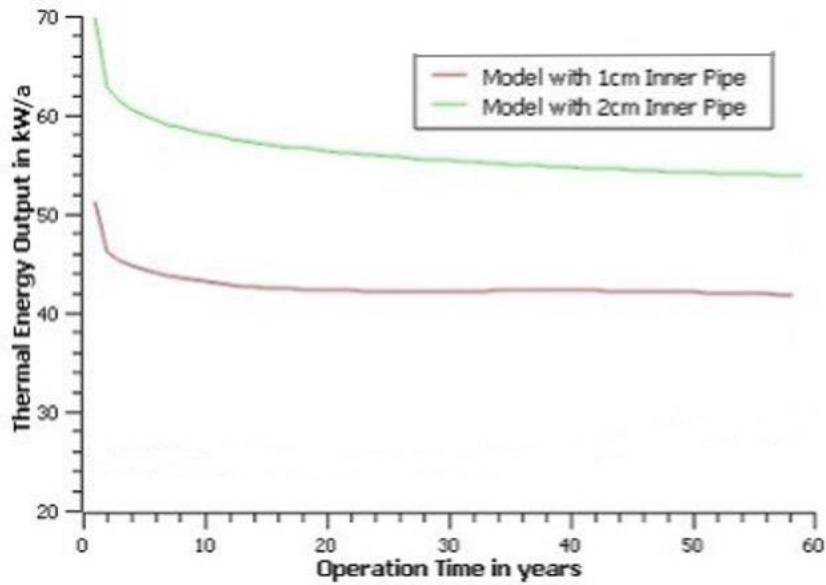


Figure 28 Variation of thermal energy output with time for models simulated in scenario 1

The variation of thermal energy output for models simulated in scenario 2 over the well lifetime is shown in Figure 29.

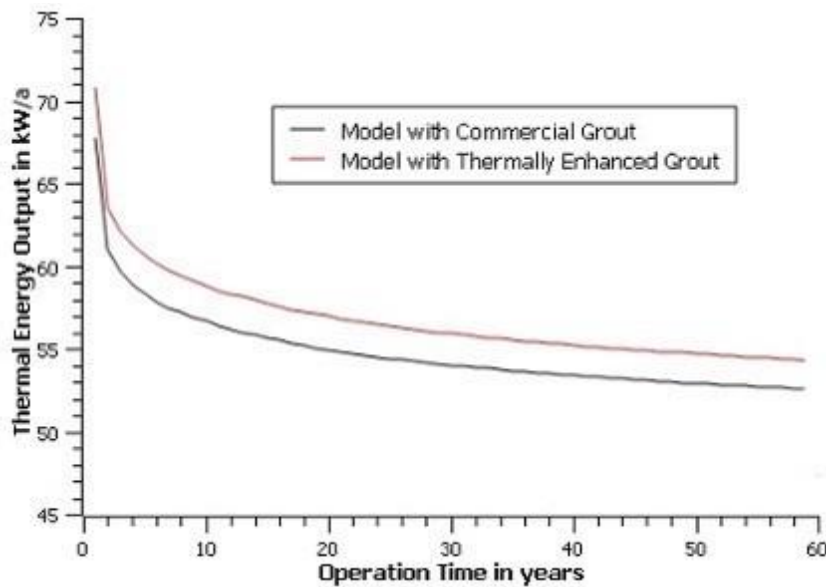


Figure 29 Variation of thermal energy output with time for models simulated in scenario 2

The variation of thermal energy output of the models with different depths of the inner pipe air gap (scenario 3) over the well lifetime is demonstrated in Figure 30.

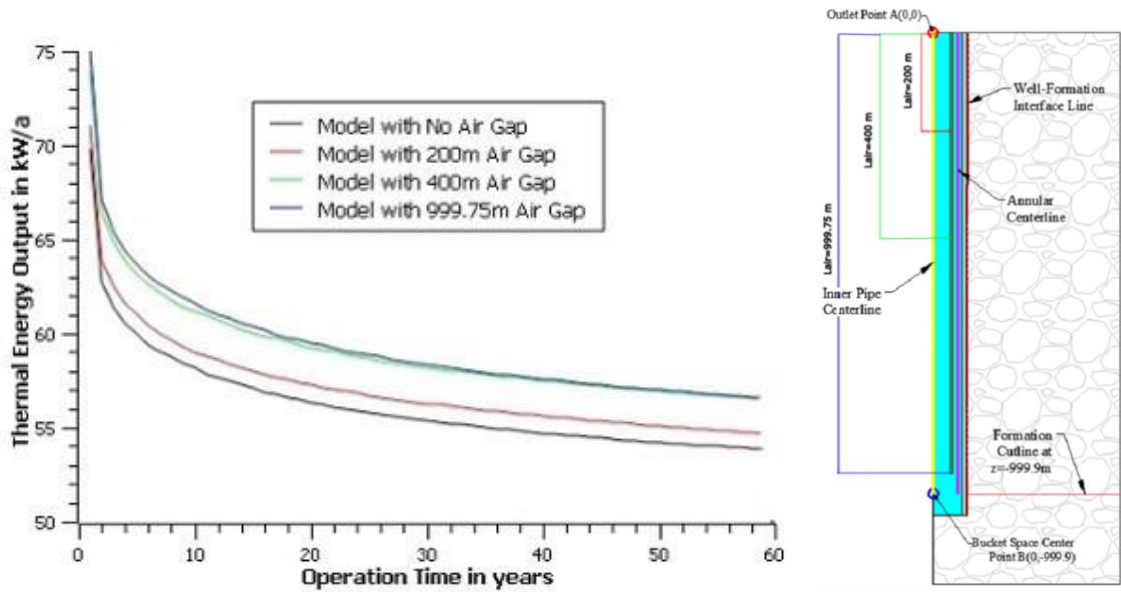


Figure 30 Variation of thermal energy output with time for models simulated in scenario 3

The models in scenario 4 (with PCM) are simulated over 60 hours and the output power is given in Figure 31. However, to compare the calculated LCOE with the other models, the thermal energy output should be estimated over 60 years. Hence, the average temperature enhancement over 60 hours is assumed to be continuous over 60 years and the LCOE is calculated accordingly. For the model with an inner pipe PCM gap of length 50 m the estimated thermal energy output is 3515.92 kW/a or 30.8 GWh compared to 29.471 GWh for a model without PCM.

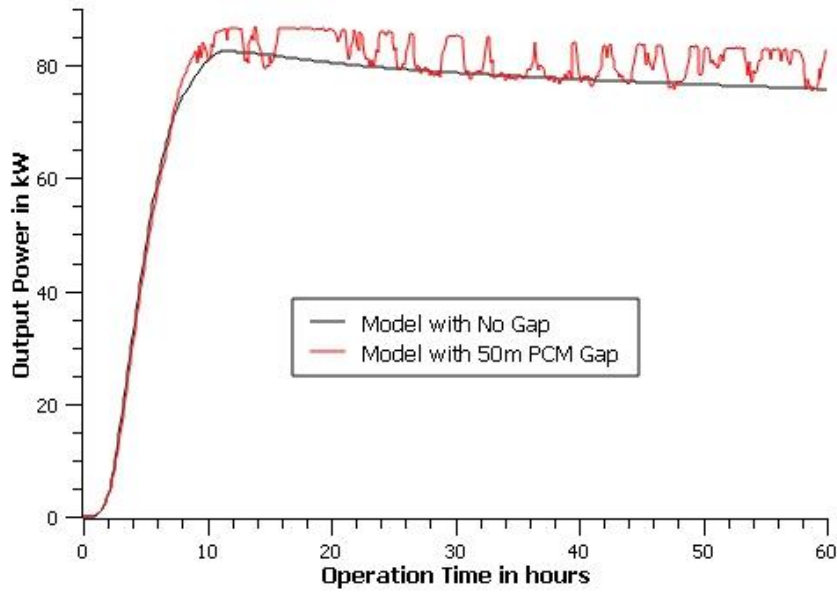


Figure 31 Variation of output power with time for models simulated in scenario 4

Assuming the lifetime of the geothermal well extends over 60 years, the overall thermal energy output of all models is listed in Table 9.

Table 9 Estimated overall thermal energy output of the simulated models

Scenario	Model	Well Lifetime (years)	Overall Thermal Energy Output (GWh)
1	Model with thin inner pipe	60	13.6
	Model with 1 cm thick pipe	60	22.375
	Model with 2 cm thick pipe*	60	29.471
2	Model with commercial grout	60	28.74
	Model with thermally enhanced grout	60	29.776
3	Model with 200 m inner pipe air gap	60	29.953
	Model with 400 m inner pipe air gap		30.995
	Model with 999.75m inner pipe air gap	60	31.104
4	Model with 50 m inner pipe PCM gap	60	30.8

(* This model is used as the base case for comparison with scenarios 2, 3, and 4)

The values of the power generated in Table 9 can be verified by the study conducted by Piipponen et al. [20], where the power produced from a 1000 m deep geothermal well was on average 65 kW which is equivalent to 569 MWh/a. Moreover, Piipponen et al. [20] reported that the maximum thermal energy production of 1000 m

deep geothermal wells in Vantaa, Jyväskylä, and Rovaniemi in Finland, are 330, 310, and 270 MWh/a, respectively.

4.4. Economic Analysis of the Models

According to the Renewable Energy Agency [49], the levelized cost of energy from any geothermal project is estimated by incorporating the capital cost of the project (i.e., cost of pipes, grout, working fluids, and other involved materials in the well). The operation and maintenance costs of the project over its entire lifetime must be added to the drilling costs of the well. Furthermore, the weighted average cost of capital (including the debt and equity of the project) is used in the LCOE calculation.

Geothermal projects development constitutes of many stages, from the pre-survey stage, exploration, test drilling, feasibility study planning, drilling and construction, startup, and finally the operation and maintenance stage that spans over the lifetime of the project. The involved costs increase when proceeding through these stages, however, the associated risks and uncertainty drop within each stage as illustrated in Figure 32.

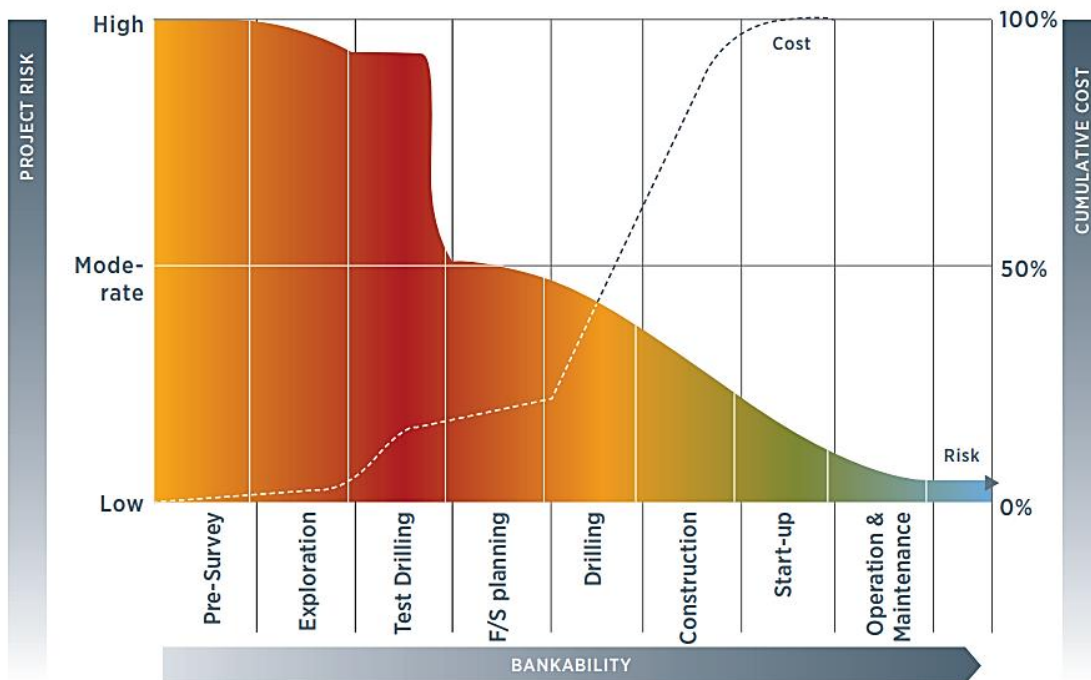


Figure 32 Common expenditure and risk profiles of any geothermal project [49], [50]

The following risks are involved in any geothermal project [50]:

- Completion/delay risk
- Financial risk
- Market demand/price risk
- Off-take risk (Risk of buyer failing to take power due to transmission line failure, dispatch, transmission congestion, or simply the inability to cover the agreed payments in a timely manner)
- Regularity risk (Risk resulting from a government's holding of discretionary power over factors influencing investor's commercial success)
- Operation risk (Risk that a geothermal facility encounters during operation phase such as equipment breakdowns)

Referring to Figure 32, the upstream phases of a geothermal project include the highest risks, these include the preliminary surveys, exploration, and the test drilling

phases. Moreover, the test drilling phase requires much more capital than the previous two phases [50]. This phase may require up to 15% of the overall capital, knowing that the project failure risk is still high during this stage.

Pan et al. [26] worked on the optimization of deep borehole heat exchangers through minimizing the average cost of energy (known as the levelized cost of energy LCOE) in \$/kWh. The project is more economically feasible with lower average cost of energy (LCOE). The LCOE includes the cost of operation and maintenance, and the materials used. For example, for the model with a PCM gap, the cost of PCM is included. Therefore, the LCOE is calculated as follows [26]

$$TC = C_{drilling\&completion} + C_{fluid} + C_{PCM} + C_{o\&m} + C_{grout} \quad (20)$$

$$LCOE = \frac{TC}{Q} \quad (21)$$

where:

LCOE: Levelized cost of energy in \$/kWh

C_{drilling&completion}: Drilling and completion costs of the well in \$

C_{grout}: Cost of the backfill material in \$

C_{fluid}: Cost of the working fluid which is water in \$

C_{PCM}: Cost of PCM deployed in the gap in \$

C_{o&m}: Operation and maintenance cost in \$

Q: Thermal energy output in kWh

TC: Total costs in \$

According to Lukawski et al. [51] the drilling and completion costs of a geothermal well is estimated (empirically) using the following equation:

$$C_{drilling\&completion} = 1.72 \times 10^{-7} \times (MD)^2 + 2.3 \times 10^{-3} \times MD - 0.62 \quad (22)$$

where:

$C_{drilling\&completion}$: Drilling and completion costs in million \$

MD : Measured depth in m

The costs described in equation (20) are listed in Table 10. The completion costs include the cost of the installed pipes (casing and tubing), in addition to the cost of conventional grout.

Table 10 Costs associated with the geothermal well model

Geothermal Well Element	Cost in \$
Well Drilling and Completion $(C_{drilling\&completion})$ (from equation (22))	1,852,000
PCM (136.33 kg) (C_{PCM}) [52]	273
Thermally Enhanced Grout (C_{grout}) [53]	7,846
Operation & Maintenance ($C_{o\&m}$) [30]	0.038 \$/kWh

The cost analysis of the well models including the total estimated costs and the levelized cost of energy is demonstrated in Table 11. The total estimated cost of the well is calculated by using equation (20). The operation and maintenance costs are calculated by multiplying the cost in \$/kWh by the overall thermal energy output (power generated) of each model in kWh. The power generated by each model is the integral of the thermal energy output curve over the well lifetime shown in Figure 28, Figure 29, and Figure 30. After calculating the total estimated cost and power generated by each model, equation (21) is used to obtain the LCOE. The LCOE values obtained fall in the range reported by the Renewable Energy Agency [49].

Table 11 Economic evaluation of the studied models

Scenario	Model	Total Estimated Cost (\$)	Power Generated over Lifetime (GWh)	LCOE (\$/kWh)
1	Model with 1cm thick pipe	2,702,250	22.375	0.12
	Model with 2cm thick pipe	2,971,898	29.471	0.1
2	Model with commercial grout	2,944,120	28.74	0.102
	Model with thermally enhanced grout	2,991,334	29.776	0.1
3	Model with 200 m inner pipe air gap	2,990,214	29.953	0.099
	Model with 400 m inner pipe air gap	3,029,810	30.995	0.097
	Model with 999.75m inner pipe air gap	3,033,952	31.104	0.097
4	Model with 50 m inner pipe PCM gap	3,022,673	30.8	0.098

4.5. Future Research Suggestions

Based on the current study, the following research is suggested to further investigate the performance of a coaxial geothermal well:

- Assess the synergy of inner pipe air gap combination with thermally enhanced grout on the well performance.
- Investigate the performance of PCM in the deeper sections of the well and over longer operation periods.
- Study the performance of PCM in the grout domain and compare with commercial and thermally enhanced grout.
- Perform a more detailed economic assessment on the studied models especially for the model with PCM.
- Study the influence of fluid flow turbulence on the well performance.

CHAPTER 5

CONCLUSION

The performance of a coaxial geothermal well is critical to the well design and to enhance the heat exchange between the formation and the working fluid and preserve the heat in the ascending working fluid for minimal heat losses. The thickness of the inner pipe has a large effect of the performance of coaxial geothermal wells. Furthermore, the utilization of thermally enhanced grout, the deployment of an inner pipe air gap and inner pipe PCM gap improved the thermal energy output of the well by 3.6%, 5.54%, and 4.51%, respectively, compared to the base case model. The suggestion to add a 400 m air gap in the inner gap has shown to enhance the well performance with minimal additional cost yielding the lowest LCOE value. This indicates that deploying an inner pipe with air gap can increase the profitability of coaxial geothermal wells. Research on the utilization of PCM in the inner pipe and in deeper sections of the well is recommended since it is believed to further enhance the well performance.

APPENDIX A

A mesh sensitivity analysis is performed and described in Table A 1 and the outlet temperature is shown in Figure A 1 for points A(0,0) and in Figure A 2 for point B(0,-999.9).

Table A 1 Results of the mesh sensitivity analyses

Mesh #	Maximum Element Size (m)	Minimum Element Size (m)	Mapped Mesh Maximum Element Size (m)	Number of Elements	Average Element Quality
Mesh 1	60	0.0075	0.03	659,517	0.891
Mesh 2	50	0.0075	0.025	794,908	0.8901
Mesh 3	40	0.0075	0.02	999,767	0.8911
Mesh 4	30	0.0075	0.015	1,341,856	0.8903
Mesh 5	25	0.0075	0.012	1,681,625	0.8902

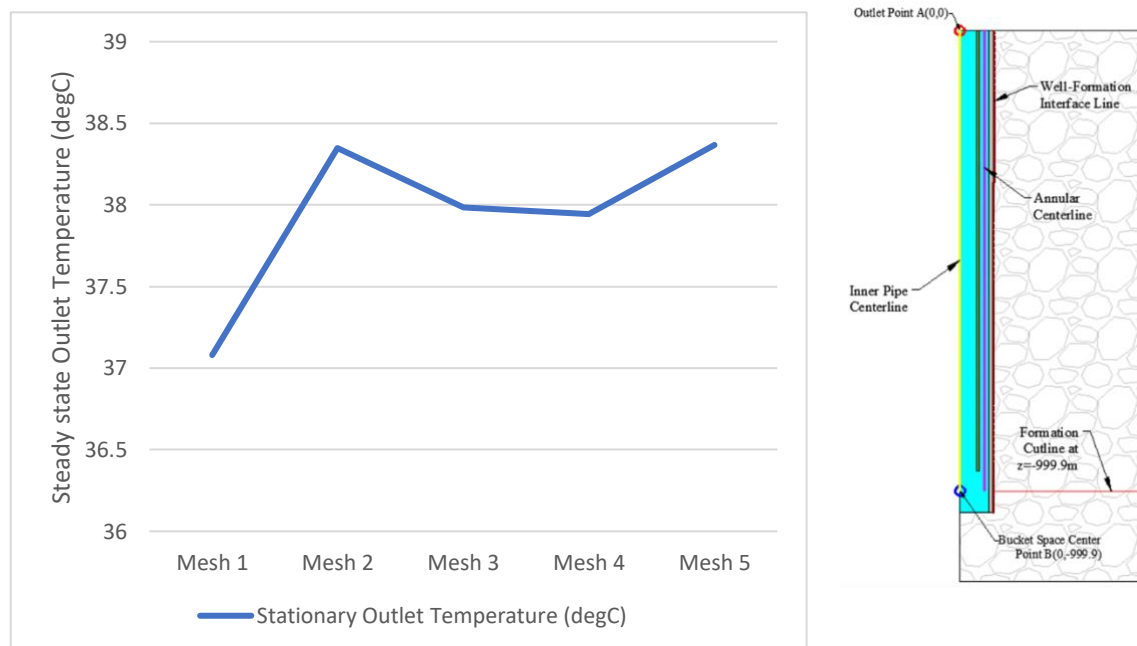


Figure A 1 Variation of the steady state outlet temperature w.r.t. number of mesh elements

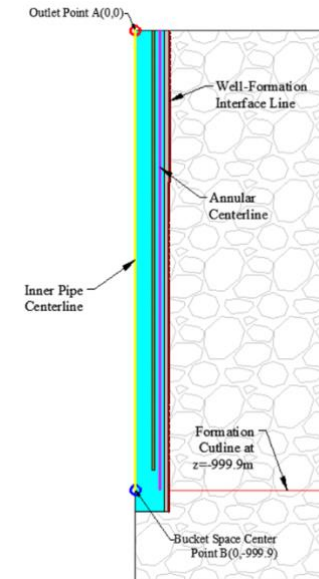
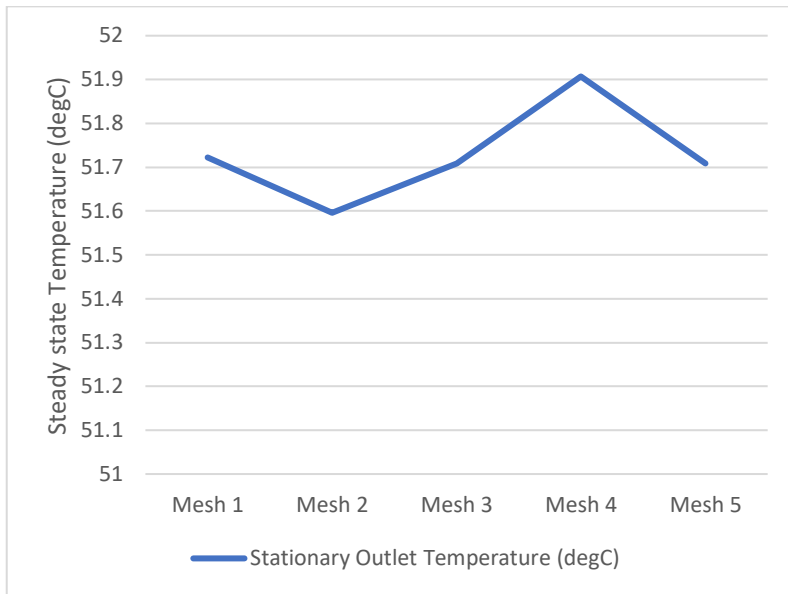


Figure A 2 Variation of the steady state temperature at point B in the bucket space w.r.t. number of mesh elements

It can be indicated that mesh 3 is the optimal mesh to work with as no significant variations in the steady state temperature of the model occurs for finer mesh elements.

REFERENCES

- [1] J. C. Kurnia, M. S. Shatri, Z. A. Putra, J. Zaini, W. Caesarendra, and A. P. Sasmito, "Geothermal energy extraction using abandoned oil and gas wells: Techno-economic and policy review," *Int J Energy Res*, vol. 46, no. 1, pp. 28–60, Jan. 2022, doi: 10.1002/ER.6386.
- [2] L. Y. Bronicki, "Introduction to geothermal power generation," *Geothermal Power Generation: Developments and Innovation*, pp. 1–3, Jan. 2016, doi: 10.1016/B978-0-08-100337-4.00001-2.
- [3] A. Budiono, S. Suyitno, I. Rosyadi, A. Faishal, and A. X. Ilyas, "A Systematic Review of the Design and Heat Transfer Performance of Enhanced Closed-Loop Geothermal Systems," *Energies 2022, Vol. 15, Page 742*, vol. 15, no. 3, p. 742, Jan. 2022, doi: 10.3390/EN15030742.
- [4] Z. Yusupov and M. Almaktar, "Geothermal Power Generation," in *Geothermal Energy*, IntechOpen, 2022. doi: 10.5772/intechopen.97423.
- [5] X. Bu, W. Ma, and H. Li, "Geothermal energy production utilizing abandoned oil and gas wells," *Renew Energy*, vol. 41, pp. 80–85, May 2012, doi: 10.1016/j.renene.2011.10.009.
- [6] R. A. Caulk and I. Tomac, "Reuse of abandoned oil and gas wells for geothermal energy production," *Renew Energy*, vol. 112, pp. 388–397, Nov. 2017, doi: 10.1016/J.RENENE.2017.05.042.
- [7] J. D. Templeton, S. A. Ghoreishi-Madiseh, F. Hassani, and M. J. Al-Khawaja, "Abandoned petroleum wells as sustainable sources of geothermal energy," *Energy*, vol. 70, pp. 366–373, Jun. 2014, doi: 10.1016/J.ENERGY.2014.04.006.
- [8] A. Chmielowska, B. Tomaszewska, and A. Sowizdzka, "The Utilization of Abandoned Petroleum Wells in Geothermal Energy Sector. Worldwide Trends and Experience," *E3S Web of Conferences*, vol. 154, p. 05004, Mar. 2020, doi: 10.1051/e3sconf/202015405004.
- [9] S. J. Zarrouk and H. Moon, "Efficiency of geothermal power plants: A worldwide review," *Geothermics*, vol. 51, pp. 142–153, Jul. 2014, doi: 10.1016/j.geothermics.2013.11.001.
- [10] A. Manzella, "Geothermal energy," *EPJ Web Conf*, vol. 148, p. 00012, Jul. 2017, doi: 10.1051/epjconf/201714800012.
- [11] Y. Zhang *et al.*, "Performance analysis of a downhole coaxial heat exchanger geothermal system with various working fluids," *Appl Therm Eng*, vol. 163, p. 114317, Dec. 2019, doi: 10.1016/J.APPLTHERMALENG.2019.114317.
- [12] H. Holmberg, J. Acuña, E. Næss, and O. K. Sønju, "Thermal evaluation of coaxial deep borehole heat exchangers," *Renew Energy*, vol. 97, pp. 65–76, Nov. 2016, doi: 10.1016/j.renene.2016.05.048.
- [13] M. Alavy, M. Peiris, J. Wang, and M. A. Rosen, "Assessment of a novel phase change material-based thermal caisson for geothermal heating and cooling," *Energy Convers Manag*, vol. 234, p. 113928, Apr. 2021, doi: 10.1016/J.ENCONMAN.2021.113928.
- [14] M. M. Mousa, A. M. Bayomy, and M. Z. Saghir, "Phase change materials effect on the thermal radius and energy storage capacity of energy piles: Experimental

- and numerical study,” *International Journal of Thermofluids*, vol. 10, p. 100094, May 2021, doi: 10.1016/J.IJFT.2021.100094.
- [15] P. Eslami-nejad and M. Bernier, “(PDF) A Preliminary Assessment on the Use of Phase Change Materials Around Geothermal Boreholes (DE-13-028),” Jan. 2013. https://www.researchgate.net/publication/268095015_A_Preliminary_Assessment_on_the_Use_of_Phase_Change_Materials_Around_Geothermal_Boreholes_DE-13-028 (accessed Nov. 20, 2022).
- [16] F. Chen, J. Mao, S. Chen, C. Li, P. Hou, and L. Liao, “Efficiency analysis of utilizing phase change materials as grout for a vertical U-tube heat exchanger coupled ground source heat pump system,” *Appl Therm Eng*, vol. 130, pp. 698–709, Feb. 2018, doi: 10.1016/J.APPLTHERMALENG.2017.11.062.
- [17] S. Barbi *et al.*, “Phase Change Material Evolution in Thermal Energy Storage Systems for the Building Sector, with a Focus on Ground-Coupled Heat Pumps,” *Polymers (Basel)*, vol. 14, no. 3, p. 620, Feb. 2022, doi: 10.3390/polym14030620.
- [18] L. Pu, L. Xu, S. Zhang, and Y. Li, “Optimization of ground heat exchanger using microencapsulated phase change material slurry based on tree-shaped structure,” *Appl Energy*, vol. 240, pp. 860–869, Apr. 2019, doi: 10.1016/j.apenergy.2019.02.088.
- [19] H. Taherian, J. L. Alvarado, K. Tumuluri, C. Thies, and C.-H. Park, “Fluid Flow and Heat Transfer Characteristics of Microencapsulated Phase Change Material Slurry in Turbulent Flow,” *J Heat Transfer*, vol. 136, no. 6, Jun. 2014, doi: 10.1115/1.4026863.
- [20] K. Piipponen *et al.*, “The deeper the better? A thermogeological analysis of medium-deep borehole heat exchangers in low-enthalpy crystalline rocks,” *Geothermal Energy*, vol. 10, no. 1, p. 12, Dec. 2022, doi: 10.1186/s40517-022-00221-7.
- [21] X. Hu, J. Banks, L. Wu, and W. V. Liu, “Numerical modeling of a coaxial borehole heat exchanger to exploit geothermal energy from abandoned petroleum wells in Hinton, Alberta,” *Renew Energy*, vol. 148, pp. 1110–1123, Apr. 2020, doi: 10.1016/J.RENENE.2019.09.141.
- [22] T. Śliwa, M. Kruszewski, A. Sapińska-Śliwa, and M. Assadi, “The application of Vacuum Insulated Tubing in Deep Borehole Heat Exchangers,” *AGH Drilling, Oil, Gas*, vol. 34, no. 2, p. 597, 2017, doi: 10.7494/drill.2017.34.2.597.
- [23] M. Mahmoud *et al.*, “A review of grout materials in geothermal energy applications,” *International Journal of Thermofluids*, vol. 10, p. 100070, May 2021, doi: 10.1016/j.ijft.2021.100070.
- [24] L. Mascarin *et al.*, “Selection of backfill grout for shallow geothermal systems: Materials investigation and thermo-physical analysis,” *Constr Build Mater*, vol. 318, p. 125832, Feb. 2022, doi: 10.1016/j.conbuildmat.2021.125832.
- [25] H. Javadi, S. Mousavi Ajarostaghi, M. Rosen, and M. Pourfallah, “A Comprehensive Review of Backfill Materials and Their Effects on Ground Heat Exchanger Performance,” *Sustainability*, vol. 10, no. 12, p. 4486, Nov. 2018, doi: 10.3390/su10124486.
- [26] S. Pan, Y. Kong, C. Chen, Z. Pang, and J. Wang, “Optimization of the utilization of deep borehole heat exchangers,” *Geothermal Energy*, vol. 8, no. 1, p. 6, Dec. 2020, doi: 10.1186/s40517-020-0161-4.

- [27] C. Alimonti, E. Soldo, D. Bocchetti, and D. Berardi, “The wellbore heat exchangers: A technical review,” *Renew Energy*, vol. 123, pp. 353–381, Aug. 2018, doi: 10.1016/j.renene.2018.02.055.
- [28] K. Morita, M. Tago, and S. Ehara, “Case Studies on Small-Scale Power Generation with the Downhole Coaxial Heat Exchanger,” *Proceedings World Geothermal Congress*, pp. 24–29, 2005.
- [29] S. Pokhrel *et al.*, “Field-scale experimental and numerical analysis of a downhole coaxial heat exchanger for geothermal energy production,” *Renew Energy*, vol. 182, pp. 521–535, Jan. 2022, doi: 10.1016/J.RENENE.2021.10.038.
- [30] N. Yildirim, S. Parmanto, and G. G. Akkurt, “Thermodynamic assessment of downhole heat exchangers for geothermal power generation,” *Renew Energy*, vol. 141, pp. 1080–1091, Oct. 2019, doi: 10.1016/J.RENENE.2019.04.049.
- [31] Y. Shi *et al.*, “Study on wellbore fluid flow and heat transfer of a multilateral-well CO₂ enhanced geothermal system,” *Appl Energy*, vol. 249, pp. 14–27, Sep. 2019, doi: 10.1016/J.APENERGY.2019.04.117.
- [32] R. A. Caulk and I. Tomac, “Reuse of abandoned oil and gas wells for geothermal energy production,” *Renew Energy*, vol. 112, pp. 388–397, Nov. 2017, doi: 10.1016/J.RENENE.2017.05.042.
- [33] M. le Lous, F. Larroque, A. Dupuy, and A. Moignard, “Thermal performance of a deep borehole heat exchanger: Insights from a synthetic coupled heat and flow model,” *Geothermics*, vol. 57, pp. 157–172, Sep. 2015, doi: 10.1016/J.GEOTHERMICS.2015.06.014.
- [34] G. Nalla, G. M. Shook, G. L. Mines, and K. K. Bloomfield, “Parametric sensitivity study of operating and design variables in wellbore heat exchangers,” *Geothermics*, vol. 34, no. 3, pp. 330–346, Jun. 2005, doi: 10.1016/J.GEOTHERMICS.2005.02.001.
- [35] S. L. Tariq, H. M. Ali, M. A. Akram, M. M. Janjua, and M. Ahmadelouydarab, “Nanoparticles enhanced phase change materials (NePCMs)-A recent review,” *Appl Therm Eng*, vol. 176, p. 115305, Jul. 2020, doi: 10.1016/j.applthermaleng.2020.115305.
- [36] A. Aljabr, A. Chiasson, and A. Alhajjaji, “Numerical Modeling of The Effects of Micro-Encapsulated Phase Change Materials Intermixed with Grout in Vertical Borehole Heat Exchangers,” *Geothermics*, vol. 96, p. 102197, Nov. 2021, doi: 10.1016/j.geothermics.2021.102197.
- [37] V. Soni *et al.*, “Evaluation of a Microencapsulated Phase Change Slurry for Subsurface Energy Recovery,” *Energy & Fuels*, vol. 35, no. 12, pp. 10293–10302, Jun. 2021, doi: 10.1021/acs.energyfuels.1c00972.
- [38] M. Kong, J. L. Alvarado, C. Thies, S. Morefield, and C. P. Marsh, “Field evaluation of microencapsulated phase change material slurry in ground source heat pump systems,” *Energy*, vol. 122, pp. 691–700, Mar. 2017, doi: 10.1016/j.energy.2016.12.092.
- [39] H. Javadi, J. F. Urchueguia, S. S. Mousavi Ajarostaghi, and B. Badenes, “Numerical Study on the Thermal Performance of a Single U-Tube Borehole Heat Exchanger Using Nano-Enhanced Phase Change Materials,” *Energies (Basel)*, vol. 13, no. 19, p. 5156, Oct. 2020, doi: 10.3390/en13195156.
- [40] X. Li, C. Tong, L. Duanmu, and L. Liu, “Research on U-tube Heat Exchanger with Shape-stabilized Phase Change Backfill Material,” *Procedia Eng*, vol. 146, pp. 640–647, 2016, doi: 10.1016/j.proeng.2016.06.420.

- [41] R. W. Pryor, *Multiphysics Modeling Using COMSOL: a First Principles Approach*. Jones and Bartlett Publishers, 2011.
- [42] M. B. Turgay and A. G. Yazıcıoğlu, “Numerical simulation of fluid flow and heat transfer in a trapezoidal microchannel with COMSOL multiphysics: A case study,” *Numeri Heat Transf A Appl*, vol. 73, no. 5, pp. 332–346, Mar. 2018, doi: 10.1080/10407782.2017.1420302.
- [43] F. Delaleux, X. Py, R. Olives, and A. Dominguez, “Enhancement of geothermal borehole heat exchangers performances by improvement of bentonite grouts conductivity,” *Appl Therm Eng*, vol. 33–34, pp. 92–99, Feb. 2012, doi: 10.1016/j.applthermaleng.2011.09.017.
- [44] P. J. Yekoladio, T. Bello-Ochende, and J. P. Meyer, “Design and optimization of a downhole coaxial heat exchanger for an enhanced geothermal system (EGS),” *Renew Energy*, vol. 55, pp. 128–137, Jul. 2013, doi: 10.1016/j.renene.2012.11.035.
- [45] D. Gordon, T. Bolisetti, D. S.-K. Ting, and S. Reitsma, “A physical and semi-analytical comparison between coaxial BHE designs considering various piping materials,” *Energy*, vol. 141, pp. 1610–1621, Dec. 2017, doi: 10.1016/j.energy.2017.11.001.
- [46] Khaled Mahmoud, Faraj Khairaldin Mohammad Khair, Faraj Jalal, Hachem Farouk, and Castelain Cathy, “A review on phase change materials for thermal energy storage in buildings: Heating and hybrid applications,” *The 6th International Conference on Emerging and Renewable Energy: Generation and Automation ICEREGA '18*, Oct. 2018.
https://www.researchgate.net/publication/329143688_A_review_on_phase_change_materials_for_thermal_energy_storage_in_buildings_Heating_and_hybrid_applications (accessed Apr. 09, 2023).
- [47] Y. He, M. Jia, X. Li, Z. Yang, and R. Song, “Performance analysis of coaxial heat exchanger and heat-carrier fluid in medium-deep geothermal energy development,” *Renew Energy*, vol. 168, pp. 938–959, May 2021, doi: 10.1016/J.RENENE.2020.12.109.
- [48] PlusICE, “Phase Change Materials: Thermal Management Solutions,” 2021. <https://www.pcmproducts.net/> (accessed Aug. 09, 2023).
- [49] I. Renewable Energy Agency, *Geothermal power: Technology brief*. 2017. [Online]. Available: www.irena.org
- [50] M. Gehringer and V. Loksha, *Geothermal Handbook: Planning and Financing Power Generation*. World Bank, Washington, DC, 2012.
- [51] M. Z. Lukawski *et al.*, “Cost analysis of oil, gas, and geothermal well drilling,” *J Pet Sci Eng*, vol. 118, pp. 1–14, Jun. 2014, doi: 10.1016/j.petrol.2014.03.012.
- [52] A. Bland, M. Khzouz, T. Statheros, and E. Gkanas, “PCMs for Residential Building Applications: A Short Review Focused on Disadvantages and Proposals for Future Development,” *Buildings*, vol. 7, no. 3, p. 78, Aug. 2017, doi: 10.3390/buildings7030078.
- [53] X. Liu, Y. Polsky, D. Qian, and J. Mcdonald, “An Analysis on Cost Reduction Potential of Vertical Bore Ground Heat Exchangers Used for Ground Source Heat Pump Systems.”